Insights into the bioluminescence systems of three sea pens (Cnidaria: Anthozoa): from *de novo* transcriptome analyses to biochemical assays

Laurent Duchatelet[1,*,$], Gabriela A. Galeazzo[2,$], Constance Coubris[1], Laure Bridoux[3], René Rezsohazy[3], Marcelo R.S. Melo[4], Martin Marek[5,6], Danilo T. Amaral[7], Sam Dupont[8,9], Anderson G. Oliveira[10], Jérôme Delroisse[11,12]

[1] Marine Biology Laboratory, Earth and Life Institute, University of Louvain – UCLouvain, Belgium
[2] Departamento de Oceanografia Física, Química e Geológica, Instituto Oceanográfico, Universidade de São Paulo, São Paulo, Brazil
[3] Animal Molecular and Cellular Biology, Louvain Institute of Biomolecular Science and Technology, University of Louvain – UCLouvain, Belgium
[4] Departamento de Oceanografia Biológica, Instituto Oceanográfico, Universidade de São Paulo, São Paulo, Brazil
[5] Loschmidt Laboratories, Department of Experimental Biology and RECETOX, Masaryk University, 625 00 Brno, Czech Republic
[6] International Clinical Research Center, St. Anne's University Hospital Brno, Pekarska 53, 656 91 Brno, Czech Republic
[7] Centre for Natural and Human Sciences, Federal University of ABC, Santo André, Brazil
[8] Department of Biological & Environmental Sciences, University of Gothenburg, Fiskebäckskil, Sweden
[9] International Atomic Energy Agency, Environment Laboratories, Principality of Monaco, Monaco
[10] Department of Chemistry and Biochemistry, Yeshiva University, 245 Lexington Ave, New York, NY 10016, USA
[11] Biology of Marine Organisms and Biomimetics, Research Institute for Biosciences, University of Mons, Belgium
[12] Cellular and Molecular Immunology, GIGA Institute, University of Liège, Belgium

* Corresponding authors: Duchatelet Laurent, Laurent.duchatelet@uclouvain.be
$ Both authors contributed equally

Abstract

Bioluminescence is the production of visible light by living organisms. It occurs through the oxidation of a luciferin substrate catalysed by luciferase enzymes. Auxiliary proteins, such as fluorescent proteins and luciferin-binding proteins, can modify the light emitted wavelength or stabilize reactive luciferin molecules, respectively. Additionally, calcium ions are crucial for the luminescence across various species. Despite the large phylogenetic distribution of bioluminescent organisms, only a few systems have been comprehensively studied. Notably, cnidarian species of the *Renilla* genus utilize a coelenterazine-dependent luciferase, a calcium-dependent coelenterazine-binding protein and a green fluorescent protein. We investigated the bioluminescence of three sea pen species: *Pennatula phosphorea*, *Anthoptilum murrayi* and *Funiculina quadrangularis* (Pennatuloidea, Anthozoa). Their light-emission spectra reveal peaks at 510, 513 and 485 nm, respectively. A coelenterazine-based reaction was demonstrated in all three species. Using transcriptome analyses, we identified predicted transcripts coding for luciferases, green fluorescent proteins and coelenterazine-binding proteins for *P. phosphorea* and *A. murrayi*. Immunodetection confirmed the expression of luciferase in *P. phosphorea* and *F. quadrangularis*. We also expressed

recombinant luciferase of *A. murrayi*, confirming its activity. We highlighted the role of calcium ions in bioluminescence, possibly associated with the mechanism of substrate release at the level of coelenterazine-binding proteins. The study proposes a model for anthozoan bioluminescence, offering new avenues for future ecological and functional research on these luminous organisms.

Keywords: Bioluminescence, Luciferase, Coelenterazine, Luciferin-binding protein, Luminous system, Pennatulidae, Anthoptilidae, Funiculidae

Introduction

Bioluminescence, the production of visible light by a living organism, involves the oxidation of a luciferin substrate catalyzed by a luciferase enzyme. In some bioluminescent systems, luciferase and luciferin form a stable complex known as "photoprotein", requiring additional co-factors to be functional [1]. Luciferases *sensu lato* (*i.e.,* luciferases *stricto sensu* and photoproteins) are classically considered taxon-specific (*i.e.,* each clade is characterized by its own luciferase) [2]. Nevertheless, homologous luciferases can sometimes be used by phylogenetically distant luminous organisms [3]. At least 12 distinct types of luciferases, *sensu lato,* have been described [3].

When the photogenic reaction occurs, the generated light is defined by a color that can differ depending on luciferin, but also on the amino acid sequence and structure of the luciferase [4-7]. In some bioluminescent organisms, light emission involves Bioluminescence Resonance Energy Transfer (BRET), a nonradiative process where a bioluminescent donor (luciferase) transfers energy to a fluorescent acceptor (fluorescent protein) [4]. The fluorescent protein absorbs photons emitted by the bioluminescence reaction and becomes excited. It then re-emits light at longer wavelengths before returning to the ground state. For example, the Green Fluorescent Protein (GFP) emits green light after absorbing blue light primarily emitted by the luciferin-luciferase reaction [1,5].

Luminous anthozoans are distributed among four orders: Actiniaria (including one luminous families), Zoantharia (including two luminous families), Malacalcyonacea (including one luminous family), and Scleralcyonacea (**Table S1**; [8]). Scleralcyonacea include 18 luminous families mainly spread into the Pennatuloidea superfamily (**Table S1**; [8]). The bioluminescence system of *Renilla reniformis* (Pallas, 1766) (Pennatuloidea) has been extensively characterized. It involves the most widespread luciferin in marine environments, the coelenterazine (6-(4-hydroxyphenyl)-2-[(4-hydroxyphenyl)methyl]-8-(phenylmethyl)-7H-imidazo[1,2-a]pyrazin-3-one), and a coelenterazine-dependent luciferase (*R*Luc-type) [9-11,14,16]. This luciferase is homologous to bacterial haloalkane dehalogenases, assumed to have been horizontally transferred during evolution [3]. In addition, more recent descriptions of similar bioluminescent molecular components in different pennatulaceans are sparse [9-17] (**Table S1**). Bessho-Uehara et al. (2020) demonstrated the widespread occurrence of coelenterazine-based *R*Luc-type luciferase across deep-sea pennatulacean species, such as *Distichoptilum gracile* (Verrill, 1882), *Umbellula* sp., *Pennatula* sp., and

Funiculina sp. [13]. In addition, *R*Luc-type luciferases have also been identified in phylogenetically distant organisms such as echinoderms (*Amphiura filiformis* (Müller, 1776) [18]), and potentially in tunicates (*Pyrosoma atlanticum* (Péron, 1804) [19]), however, this has recently been called into question [20]. Luminescence-associated molecules, such as coelenterazine-binding proteins (CBPs) and GFPs have also been identified in sea pansy and other pennatulaceans [16,21-26]. Additionally, the calcium ion has been demonstrated to be indirectly involved in light production in *R. reniformis* and *Veretillum cynomorium* (Pallas, 1766) [27,28]. CBP relies on calcium ions as cofactors to release luciferin, enabling light production in *R. reniformis* [29].

Light production in sea pens occurs within specific endodermal cells (*i.e.,* photocytes), depending on the species, in the tissues of autozooid and siphonozooid polyps [30-32]. These photocytes often exhibit green autofluorescence [33,34]. To date, bioluminescent pennatulaceans display nervous catecholaminergic control of light emission, with adrenaline- and noradrenaline-triggered waves of light flashes [35,36]. Although no experimental behavioral evidence has been obtained, the ecological function of pennatulacean luminescence may serve as an aposematic signal, avoiding predation through misdirection or burglar alarm effects [2,37]. The current data and gaps in the anthozoan bioluminescence data are presented in **Table S1**.

Although the *Renilla* bioluminescence system has been extensively characterized, the molecular mechanisms and components involved in the bioluminescence of other sea pen species remain largely unexplored. This study aimed to explore the unique bioluminescent systems of three sea pen species, the pennatulid *Pennatula phosphorea* (Linnaeus, 1758), funiculinid *Funiculina quadrangularis* (Pallas, 1766), and anthoptilid *Anthoptilum murrayi* (Kölliker, 1880), focusing on their biochemical and molecular aspects. A multidisciplinary study using luminometric assays, transcriptome and phylogenetic analyses, 3D protein modeling, and immunodetection revealed the basis of the bioluminescent system of these soft coral sea pens. Cross-reaction luminometric results highlight the involvement of a *R*Luc-like luciferase in *P. phosphorea* and *F. quadrangularis*, both shallow water species, with coelenterazine as the substrate for all three bioluminescent systems. Besides, *P. phosphorea* and *A. murrayi de novo* transcriptome analyses corroborate (*i*) the homology of both retrieved luciferase sequences with the *Renilla* luciferase, (*ii*) the *in silico* presence of multiple CBPs-like and GFPs-like proteins homologous to the functionally characterized references proteins . The luciferase expression sites within the autozooids and siphonozooids of *P. phosphorea* and autozooids of *F. quadrangularis* are described. The presence of GFP was also strongly suggested in *P. phosphorea* through comparative microscopy. Finally, the pharmacological involvement of calcium in the light emission process of *P. phosphorea* and *F. quadrangularis* is confirmed.

Materials and methods

Specimen collection

In July 2022 and 2023, common sea pens (*Pennatula phosphorea*, n = 30), were collected from the Gullmarsfjord, Sweden, using a small dredge with a 1 m aperture at a depth of 35–40 m. Likewise, tall sea pens (*Funiculina quadrangularis*, n = 11), were sampled in July 2023 using the same method at a depth of 40 m. Animals were transported to the Kristineberg Marine Research Station (Fiskebäckskil, Sweden) and maintained under dark condition in a continuous flow of fresh deep-sea water pumped from the adjacent fjord.

Specimens of Murrays' sea pens (*Anthoptilum murrayi*, n = 3) were collected during the DEEP-OCEAN expedition off the southeast coast of Brazil aboard the R/V Alpha Crucis. The collection was carried out using a demersal trawl net with 19 m lower rope, mesh sizes of 100 mm in the body and wings, and 25 mm in the codend, at an average depth of 1,500 m. Collection permits were issued by the *Instituto Chico Mendes de Conservação da Biodiversidade* (SISBIO permits #28054-4, 82624-1) and the *Secretaria da Comissão Interministerial para Recursos do Mar da Marinha do Brasil* (Portaria No. 223). After hoisting the net, all collected organisms were sorted, and *A. murrayi* specimens were promptly frozen in liquid nitrogen. These samples were stored at -80 °C at the Oceanographic Institute of the University of São Paulo (São Paulo, Brazil).

Dissection & sample preparation

Specimens of *P. phosphorea* and *F. quadrangularis* were anesthetized by immersion in 3.5% $MgCl_2$ solution in sea water for 30 minutes [36]. For each tested specimen of *P. phosphorea*, (*i*) the pinnules were dissected and weighed, and (*ii*) the rachis was divided into three equivalent portions and weighed. For specimens of *F. quadrangularis*, the rachis bearing the polyps was cut into 3 cm-long segments. Sea pen pinnules and rachises were either used directly for biochemical assays or rinsed for 3 h in fresh, running deep-sea water for pharmacological calcium assays. Other specimens were fixed in 4% paraformaldehyde (PFA) in phosphate buffer saline (PBS, 123 mM NaCl, 2.6 mM KCl, 12.6 mM Na_2HPO_4, 1.7 mM KH_2PO_4, pH 7.4) for subsequent immunodetection techniques.

Due to the challenges of collecting organisms from great depths (e.g., trawling damage), maintaining the survival of *A. murrayi* was not feasible. Consequently, all measurements were conducted on frozen samples.

In vivo *and* in vitro *light emission spectrum of* Anthoptilum murrayi

The bioluminescence spectrum of *A. murrayi* was obtained using frozen coral pieces thawed and hydrated with deionized water. The spectra were recorded using a cooled CCD camera (LumiF SpectroCapture AB-1850). Measurements were conducted in triplicate, with an exposure time of 2 min at room temperature.

Similarly, the emission spectrum of the recombinant *A. murrayi* luciferase was recorded on the same equipment over a 60-second interval. Prior to this, the candidate *A. murrayi* luciferase coding sequence (obtained based on the method "*De novo transcriptome analyses for Pennatula phosphorea and Anthoptilum murrayi*" section) was optimized for *E. coli* expression and cloned into the pET-28a vector (Biomatik) between the BamHI and

HindIII restriction sites. The N-terminal His-tagged luciferase was expressed in *E. coli* BL21 (DE3) cells, induced with 1 mM IPTG at 15°C overnight. Cells were harvested and lysed in 50 mM sodium phosphate buffer (pH 7.4) containing lysozyme. The lysate was then purified using Ni-NTA affinity chromatography with an imidazole gradient (100–500 mM). Final luciferase preparations were pooled, dialyzed against 50 mM sodium phosphate buffer (pH 7.4), screened for light emission activity, and concentrated using a 3-kDa cutoff filter (Vivaspin 500, GE Healthcare). Unless otherwise stated, protein concentrations were measured using a Qubit 3.0 fluorometer (Invitrogen). The luminescent reaction was then conducted under conditions identical to the standard light emission assay. Specifically, 100 µL of solution containing *A. murrayi* luciferase was diluted with 397 µL of 50 mM phosphate buffer (pH 7.4). The reaction was then initiated by adding 2 µL of native coelenterazine, bringing the total volume to 500 µL and yielding a final coelenterazine concentration of 6 µM.

Luminescent system biochemistry

Eleven specimens of *P. phosphorea* were used for biochemical analysis. Tests were performed for the pinnules (n = 40), rachises (n = 10), and peduncles (n = 10). Pinnule locations along the axis were observed and classified as upper, middle, and lower, depending on the attachment position on the rachis, as in Duchatelet et al., 2023 [36]. Five specimens of *F. quadrangularis* were used immediately after dissection for biochemical assays. Measurements were performed independently of the polyp-bearing rachis location among the colonies (n = 10). Deep-frozen tissues from two *A. murrayi* specimens were used for this analysis. For the first two species, the central rigid calcified axis of the rachis was removed before starting experiments.

Light emission measurements were performed in a dark room using an FB12 tube luminometer (Tirtertek-Berthold, Pforzheim, Germany) calibrated with a standard 470 nm light source (Beta light, Saunders Technology, Hayes, UK). Light responses were recorded using FB12-Sirius PC Software (Tirtertek-Berthold). Light emission was characterized as follows: (*i*) maximum light intensity (Lmax), expressed in megaquanta per second (10^9 q s^{-1}), and (*ii*) total amount of light emitted (Ltot) over 3 min, expressed in megaquanta. All data were standardized per unit mass (g).

Luciferase and coelenterazine assays in Pennatula phosphorea, Anthoptilum murrayi and Funiculina quadrangularis

For the luciferase assay, *P. phosphorea* pinnule and rachis and *F. quadrangularis* rachis were placed in 200 µl of Tris buffer (20 mM Tris, 0.5 mM NaCl; pH 7.4) and crushed with mortar and pestle until a homogenized extract was obtained; 20 and 40 µl of the extract was diluted in 180 and 160 µl Tris buffer, respectively. The diluted *P. phosphorea* and *F. quadrangularis* luciferase solutions were injected into two different tubes filled with 5 µl of a 1/200 stock solution of coelenterazine (Prolume Ltd., Pinetop, AZ, USA) in cold methanol (1OD at 430 nm) diluted in 195 µl of Tris buffer. Two measurements of Lmax were recorded

and averaged to calculate the maximal light decay rate corresponding to luciferase activity expressed in 10^9 q s^{-1} g^{-1} [1].

For coelenterazine detection, *P. phosphorea* pinnules, rachises, and *F. quadrangularis* rachises were placed in 200 µl of cold argon-saturated methanol and crushed using a mortar and pestle. Then, 5 µl of the methanolic extract was injected into a tube filled with 195 µl of Tris buffer and placed in a luminometer. Afterwards, 200 µl of *Renilla* luciferase solution constituted 4 µl of *Renilla* luciferase (Prolume Ltd., working dilution of 0.2 g l^{-1} in a Tris-HCl buffer 10 mM, NaCl 0.5 M, BSA 1%; pH 7.4) and 196 µl of Tris buffer was injected into the luminometer tube. The Ltot was recorded and used to calculate the amount of coelenterazine contained in a gram of pinnule (ng g^{-1}), assuming that 1 ng of pure coelenterazine coupled with *Renilla* luciferase emits 2.52×10^{11} photons [1].

A. murrayi tissues were processed using a Potter-Elvehjem homogenizer in 2 mL of Tris-HCl buffer (50 mM, pH 8.0). Following homogenization, the mixture was centrifuged at 15,000 × g for 10 min at 4°C and the pellet was discarded. The supernatant was used for the light emission assays. For each assay, the mixture comprised 100 µL of supernatant, 397 µL of Tris-HCl buffer (50 mM, pH 7.4), and 3 µL of coelenterazine (Prolume Ltd., Pinetop, AZ, USA), to achieve a final volume of 500 µL with a final concentration of 6 µM.

Control measurements were performed using coelenterazine in the presence of the buffer, and the emitted light remained around 1,000 RLU. This value was subtracted from the light emitted by the enzymatic assays for standardization purposes. All luminescence assays were conducted in triplicate, and the final result represents the average of the triplicates.

Long-term light monitoring of coelenterazine production in Pennatula phosphorea

The *P. phosphorea* specimens (n = 12) were maintained in tanks filled with circulating artificial seawater (ASW; 400 mM NaCl, 9.6 mM KCl, 52.3 mM $MgCl_2$, 9.9 mM $CaCl_2$, 27.7 mM Na_2SO_4, 20 mM Tris; pH 8.2) at temperatures following natural temperature variations encountered in the native fjord (https://www.weather.mi.gu.se/kristineberg/en/data.shtml) with a 12-12 hours photoperiod. Sea pens were fed weekly with REEF LIFE Plancto (Aqua Medic, Germany), a food without any coelenterazine trace. After six and 12 months, potassium chloride (KCl) depolarization, coelenterazine content, and luciferase activity assays were performed on eight and four specimens, respectively, with two replicates per specimen. Luciferase and coelenterazine assays were performed as previously described. Total depolarization through KCl application allows for rapid estimation of the luminous ability of specimens. For the KCl experiments, luminescence induction was performed on the pinnule and rachis portions placed in a tube luminometer filled with 500 µL of ASW. Then, the light emission was triggered with the addition of 500 µL of a KCl solution (400 mM KCl, 52.3 mM $MgCl_2$, 9.9 mM $CaCl_2$, 27.7 mM Na_2SO_4, 20 mM Tris; pH 8.2), and Ltot was recorded over 3 minutes. The recorded luciferase activity, luciferin content, and KCl response were compared with wild-caught measurements.

De novo *transcriptome analyses for* Pennatula phosphorea *and* Anthoptilum murrayi

The pinnule, rachis, and peduncle tissues of a single *P. phosphorea* specimen were dissected and directly immersed in a permeabilizing RNAlater-Ice (Life Technologies) solution overnight at -20°C, following the manufacturer's protocol. Subsequently, the samples were stored at -80°C and processed for RNA extraction. Total RNA was extracted using the TRIzol reagent. The quality of the RNA extracts (RIN value, fragment length distribution, and 28S/18S ratio) and their concentrations were assessed using an Agilent 2100 bioanalyzer. The BGI company (Beijing Genomics Institute, Hong Kong) performed cDNA library preparation and sequencing using a procedure similar to that previously described [38-40]. High-throughput sequencing was conducted using the BGISEQ-500 platform to generate 100 bp paired-end reads. To exclude low-quality sequences, the raw reads were filtered by removing (*i*) reads with more than 20% of the qualities of the base lower than 10, (*ii*) reads only containing the adaptor sequence, and (*iii*) reads containing more than 5% of unknown nucleotide "N." Quality control of the reads was performed using FastQC software [41]. For *P. phosphorea,* a reference *de novo* transcriptome assembly was then created from the remaining clean reads obtained from the pinnule, rachis, and peduncle tissues using Trinity software [42] (Trinity-v2.5.1; min_contig_length 150, CPU 8, min_kmer_cov 3, min_glue 3, SS_lib_type RF, bfly_opts'-V 5, edge-thr=0.1, stderr'). TGICL software was then used to reduce transcriptome redundancy by assembling the contigs into a single set of longer, non-redundant, and more complete consensus unigenes [43] (Tgicl-v2.5.1; -l 40 -c 10 -v 25 -O '-repeat_stringency 0.95 -minmatch 35 -minscore 35'). Unigenes, defined as non-redundant assembled sequences obtained from assembly and/or clustering [44], can form clusters in which the similarity among overlapping sequences is greater than 70% or singletons that are unique unigenes. For all transcriptomes, unigene expression was evaluated using the "Fragments per kilobase of the transcript, per million fragments sequenced" (FPKM) method [38-40,44]. To obtain annotation for transcriptomes, unigenes were aligned to NCBI Nucleotide (NT), NCBI protein (NR), EuKariotic Orthologous groups (KOG), Kyoto Encyclopedia of Genes and Genomes (KEGG), and UniProtKB/Swiss-Prot databases using Blastn, Blastx [45], and Diamond [46]. Blast2GO [47] with NR annotation results was used to obtain Gene Ontology annotations according to molecular function, biological process, and cellular component ontologies. InterPro [48] was also used to annotate unigenes based on functional analyses of protein sequences, clustering them into families and predicting the presence of domains or essential amino acid residues. The candidate coding area among the unigenes was assessed using Transdecoder (https://transdecoder.github.io).

A similar procedure was used for the specimen of *A. murrayi*. Whole sea pen tissues (pinnule and peduncle) were dissected, frozen in liquid nitrogen, and stored at -80°C. The total RNA from the sea pen was extracted using the RNeasy Plant Mini Kit (QIAGEN), following the manufacturer's instructions. RNA samples were treated with DNase I (Invitrogen) to remove potential genomic DNA contamination. Subsequently, to remove impurities and residual DNase I reaction remnants, they underwent a column cleanup process, following the instructions of the QIAGEN Kit. The concentrations of RNA samples

292 were estimated by fluorescence using a Qubit fluorometer (Thermo Fisher Scientific). The
293 integrity of the RNA samples was confirmed by agarose gel electrophoresis (1%) stained with
294 SYBR Safe (Invitrogen), and the RNA was dried at 30°C for 1 h in speed vac mode V-AQ.
295 The quality of RNA extracts (RIN value, fragment length distribution, and 28S/18S
296 ratio) and their concentration were assessed by RNA concentrations were evaluated using
297 an Agilent 2100 bioanalyzer. After QC, mRNA was enriched using oligo(dT) beads. First,
298 mRNA was randomly fragmented by adding a fragmentation buffer. Then, the cDNA was
299 synthesized using an mRNA template and random hexamer primer, after which a custom
300 second-strand synthesis buffer (Illumina), dNTPs, RNase H, and DNA polymerase I were
301 added to initiate second-strand synthesis. After a series of terminal repairs, A ligation, and
302 sequencing adaptor ligation, the double-stranded cDNA library was completed through size
303 selection and PCR enrichment. The GenOne Biotechnologies company (Brazil) performed
304 cDNA library preparation and sequencing (150 bp paired-end reads). To exclude low-quality
305 sequences, the raw reads were filtered by removing (*i*) reads with more than 50% of the
306 qualities of the base lower than 5, (*ii*) reads only containing the adaptor sequence, and (*iii*)
307 reads containing more than 10% of unknown nucleotide "N."
308 RNA sequencing was performed with v4 2×100 bp reads on the HiSeq2500
309 platform by NGS Soluções Genômicas in Piracicaba, São Paulo. The reference *de novo*
310 transcriptome assembly was generated using Trinity v2.13.2. To differentiate among
311 identified isoforms, transcript abundance was analyzed using the
312 *align_and_estimate_abundance.pl* script from the Trinity software package [49].
313 Transcriptome completeness was evaluated using BUSCO v4 (Benchmarking
314 Universal Single-Copy Orthologs), a bioinformatics tool that determines the proportion of
315 single-copy orthologs present in the dataset Metazoa_odb9. The BUSCO analysis and
316 visualization of the results were conducted on the Galaxy platform (https://usegalaxy.org).
317
318 *Light emission process-related protein sequence analyses*
319 Potential transcripts of interest were chosen using NCBI online tools according to
320 potential phylogenetic homologies to identify genes involved in the light production process,
321 such as luciferases, green fluorescent proteins, and coelenterazine-binding proteins. These
322 "light emission process-related genes" were searched within the newly generated *P.*
323 *phosphorea* transcriptome using tBLASTn analysis (1 hit, E-value < $1e^{-20}$). All retrieved
324 unigenes were individually reciprocally searched in the NCBI NR database (Reciprocal
325 BLASTx; 1hit, E-value < $1e^{-20}$). BLAST hits with significant E-values strongly support
326 homologous proteins. *In silico* translation (ExPASy translate tool,
327 http://expasy.org/tools/dna.html) was performed on the sequences retrieved from the *P.*
328 *phosphorea* and *A. murrayi* transcriptomes for all putative candidates. Multiple alignments
329 were performed for each predicted protein with their respective homologous "light emission
330 process-related protein" retrieved from the NCBI online tool in other species using Geneious
331 software [50]. Sequence alignments have enabled the identification of luciferase
332 characteristic features, such as catalytic triads [51].

333 To validate the *P. phosphorea* luciferase retrieved sequence, primers were designed
334 based on *Renilla muelleri* luciferase mRNA (AY015988.1) to amplify the hypothetical
335 luciferase sequence using Primer Blast software (**Table S2**). *P. phosphorea* pinnules were
336 collected and lysed in 300 µL of 50 mM NaOH for 30 min at 95°C with agitation at 800 rpm.
337 The pH was adjusted by adding 60 µL 500 mM Tris-HCl at pH 8. For PCR amplification, the
338 reaction mix contained 1U of Expand Long Template (Roche) with the provided buffer, 400
339 µM dNTP (#R0191, Life Technologies), and 250 nM of each primer. Amplification was
340 performed as follows: 95°C for 5 min; 35 cycles of denaturation at 95°C for 30 s,
341 hybridization from 52 °C to 55°C for 15 s, and elongation at 68°C for 45–80 s. The final cycle
342 was completed with a final elongation step at 68°C for 7 min. Primer pairs F1-R1, F2-R2, and
343 F8-R2 resulted in amplifications visualized through electrophoresis and ethidium bromide
344 incorporation. Genomic DNA was purified using the Qiagen PCR Purification Kit according to
345 the manufacturer's instructions and sequenced by Microsynth.
346
347 *Phylogenetic analyses*
348 The predicted sequences of the luciferases (LUC), GFP, and CBPs of *P. phosphorea*
349 and *A. murrayi* were placed into an anthozoan-focused phylogenetic context using maximum
350 likelihood phylogenetic reconstruction [52]. *Renilla*-type luciferase sequences from selected
351 metazoans were collected from public databases based on literature [13,17,18]. GFP
352 sequences from cnidarians were collected from public databases using reference literature
353 [53-56]. CBP sequences from anthozoans were collected from public databases based on
354 literature [57]. Multiple alignments of all sequences were performed using the MAFFT
355 algorithm implemented in the Geneious software and trimmed using TrimAL software [58].
356 Maximum likelihood phylogenetic analyses were performed using IQ-tree software [59].
357 Before the analyses, ModelTest [60] was used to select the best-fit evolution model. Trees
358 were edited using the iTOL web tool.
359
360 *Structural modeling*
361 AlphaFold models of *P. phosphorea* and *A. murrayi* LUC, GFP, and CBP proteins were
362 obtained from the AlphaFold web server (https://alphafoldserver.com/). The structural
363 models were visualized using PyMOL 2.6 (https://pymol.org/). Structural pairwise alignments
364 and calculations were performed using the Dali server
365 (http://ekhidna2.biocenter.helsinki.fi/dali/).
366
367 *Luciferase and green fluorescent protein immunodetection*
368 Commercial antibodies against *Renilla* luciferase (GTX125851, Genetex) were used to
369 confirm the presence of a *Renilla*-like luciferase. Proteins were extracted from frozen
370 pinnules, rachis, and peduncle samples. Each sample was homogenized on ice in 1000 µl of
371 2% Triton X-100 in phosphate buffer saline (PBS: 10 mM Tris, pH 7,5; 1 mM EDTA, pH 8,0;
372 100 mM NaCl) supplemented with protease inhibitors (complete–Mini tablets, Roche). The
373 extract was sonicated and centrifuged at 800 g for 15 min. The supernatant was then

374 collected. The protein concentration in each extract was measured using a PierceTM BCA
375 Protein Assay Kit (Thermo Scientific). Laemmli buffer (Bio-Rad) and β-mercaptoethanol
376 (βMSH, Bio-Rad) were added to each protein extract and the proteins were
377 electrophoretically separated at 200 V for 35 min on 12% SDS-PAGE gels. The separated
378 proteins were electroblotted onto nitrocellulose membranes. The membrane was incubated
379 overnight with the primary anti-*Renilla* luciferase antibody and the secondary antibody (ECL
380 HRP-conjugated anti-rabbit antibody, Life Sciences, NA934VS, lot number 4837492) for 1 h.
381 Antibody detection was performed using the reagents of the detection kit (HRP Perkin-
382 Elmer, NEL 104) following the manufacturer's instructions. The dilution for the primary
383 antibody was 1:2000.
384 The same primary antibody was used to immunolocalize luciferases within the *P.*
385 *phosphorea* pinnules, rachis, peduncle tissues, and *F. quadrangularis* polyp tissue. For *whole-*
386 *mount* immunofluorescence, the dissected samples were blocked with PBS containing 2%
387 Triton X-100 and 6% BSA (Amresco). Samples were then incubated for 48 h with either the
388 anti-*Renilla* luciferase antibody diluted 1:200 in PBS containing 1% Triton X-100, 0.01% NaN_3,
389 and 6% BSA. Visualization of the luciferase signal was performed after 24 h of incubation of
390 the samples at RT in the dark with a fluorescent dye-labeled secondary antibody (Goat Anti-
391 Rabbit, Alexa Fluor 594, Life Technologies Limited) diluted 1:500 in PBS containing 1% Triton
392 X-100, 0.01% NaN_3, and 6% BSA. Samples were mounted (Mowiol 4–88, Sigma) and
393 examined using an epifluorescence microscope (Axio Observer, Zeiss, Oberkochen,
394 Germany) equipped with Zen microscopy software (Zeiss, Oberkochen, Germany). Control
395 sections were incubated in PBS containing 1% Triton X-100, 0.01% NaN_3, and 6% bovine
396 serum albumin (BSA) with no primary antibodies.
397
398 *Calcium assays*
399 Following the identification of the key proteins involved in the luminescence system,
400 we assessed the role of calcium, another crucial element in the bioluminescence
401 mechanism. Different pharmacological tests were used to investigate the role of calcium in
402 the light-emission process of *P. phosphorea* and *F. quadrangularis* (n = 6 for each species).
403 First, the calcium concentration was tested using three artificial seawater (ASW) solutions
404 with different calcium concentrations (0, 10, and 20 mM $CaCl_2$). To remove any traces of Ca^{2+}
405 ions in the 0 mM $CaCl_2$ -ASW solution, calcium chelators EGTA (4100, Merck) and BAPTA
406 (14513, Merck) were added to the solution at 10^{-5} M final concentrations. Secondly, the
407 effect of a calcium ionophore (A23187; C7522, Merck) was tested to highlight the potential
408 involvement of calcium storage in the light emission process. Third, the involvement of
409 calcium was tested in the presence of a previously determined triggering agent of light
410 emission in sea pens, adrenaline at 10^{-5} M. Finally, calcium involvement was tested on the
411 effect of the potassium chloride depolarization solution usually employed to trigger the
412 maximum light production in a bioluminescent species.
413 After rinsing for 3 h, the pinnules of *P. phosphorea* and polyp-bearing rachises of *F.*
414 *quadrangularis* were placed in luminometer tubes and subjected to various treatments

415 (**Table S3**). Before the experiments, each sample was pre-incubated for 15 min in ASW
416 devoid of calcium (0 mM $CaCl_2$). Data were recorded for 15 minutes using an FB12 tube
417 luminometer (Tirtertek-Berthold, Pforzheim, Germany). Light emission was defined as the
418 total amount of light emitted (L_{tot}) over 15 min, and was expressed in megaquanta. All data
419 were standardized per unit mass (g).
420
421 *Statistical analysis*
422 All statistical analyses were performed with R Studio (version 2023.03.1 + 446, 2022,
423 Posit Software, USA). Variance normality and equality were tested using the Shapiro–Wilk
424 test and Levene's test, respectively. When these parametric assumptions were met,
425 Student's t-test and ANOVA coupled with Tukey's test were used to perform single or
426 multiple comparisons between groups. When log transformation did not provide normality
427 and homoscedasticity, the nonparametric Wilcoxon test and Kruskal–Wallis test coupled
428 with the Wilcoxon rank-sum test were used to assess whether significant differences were
429 present between the two groups or multiple groups. Differences were considered significant
430 at a minimum *p-value* of < 0.05. Values are graphically illustrated as the mean and standard
431 error of the mean (s.e.m).
432
433 **Results**
434
435 **Pennatula phosphorea*,* Funiculina quadrangularis*, and* Anthoptilum murrayi *emit light***
436 ***using a coelenterazine-dependent luciferase.***
437
438 Biochemical assays performed on *P. phosphorea*, *F. quadrangularis*, and *A. murrayi*
439 (**Figures 1A-F**) demonstrated a similar response pattern. The cross-reactivity of the extracts
440 with the commercial *Renilla* luciferase highlights the involvement of coelenterazine in the
441 bioluminescent systems of *P. phosphorea*, *F. quadrangularis*, and *A. murrayi* (**Figure 1**). For
442 *P. phosphorea*, the measured amounts of coelenterazine present no statistical differences
443 between the pinnule areas (ANOVA, *p-value* lower-middle = 0.8122; *p-value* lower-upper =
444 0.9054; *p-value* upper-middle = 0.7014) (**Figure S1**). Similarly, no significant differences were
445 observed between the rachis portions (ANOVA, *p-value* lower-middle = 0.5905; *p-value*
446 lower-upper = 0.8274; *p-value* upper-middle = 0.4634) (**Figure S1**). The mean coelenterazine
447 content per pinnule and rachis were 131.15 ± 29.06 and 70.00 ± 16.79 ng g^{-1}, respectively.
448 Peduncle presents an almost negligible mean value of 0.21 ± 0.01 ng g^{-1}. Comparatively, the
449 mean coelenterazine content of *F. quadrangularis* polyp-bearing rachis was 3.79 ± 1.20 ng g^{-}
450 ^{1}.
451

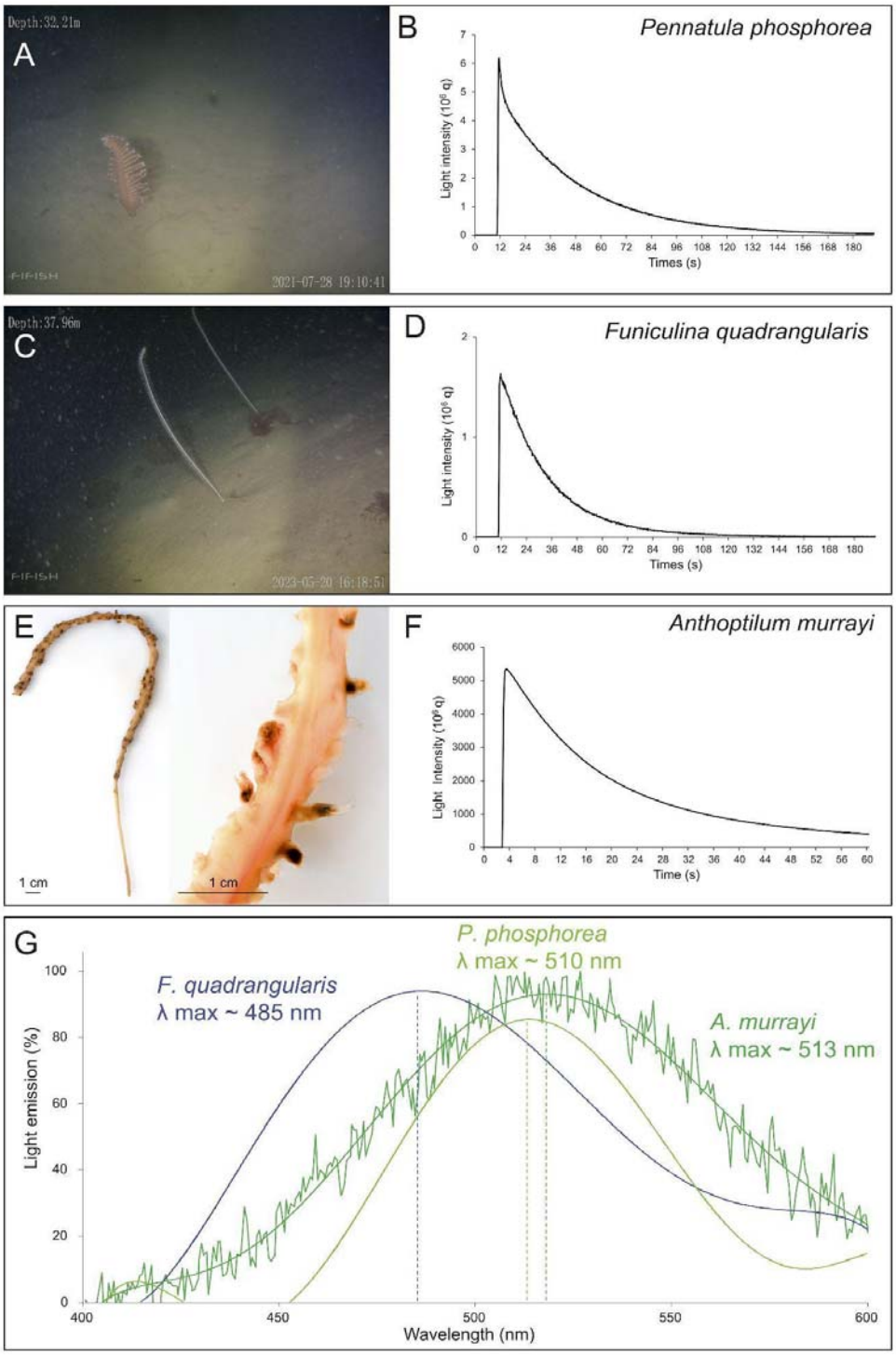

Figure 1. Biochemistry assays. (A) *In situ* images of *Pennatula phosphorea* and (B) typical coelenterazine assay curve for the pinnules. (C) *In situ* images of *Funiculina quadrangularis* and (D) typical coelenterazine assay curve for the 3 cm-long polyp-bearing rachis. (E) Images of *Anthoptilum murrayi* with a zoom on the polyp on the rachis and (F) typical coelenterazine assay curve for the whole specimen. (G) *Anthoptilum murrayi in vivo* luminescence spectrum compared with the retrieved spectrum of two other species (*P. phosphorea* [61] and *F. quadrangularis* [13]). Pictures (A and C) were provided by Fredrik Gröndahl.

In parallel, a typical coelenterazine assay curve was observed for all three species (**Figures 1B, D, and F)**. Cross-reaction assays using synthetic coelenterazine to measure potential luciferase activity confirmed the involvement of a coelenterazine-based luciferase system in *P. phosphorea* and *F. quadrangularis*. For *P. phosphorea*, luciferase activities in the pinnules show no statistically significant differences across the pinnule areas (ANOVA, *p-value* lower-middle = 0.4963; *p-value* lower-upper = 0.2742; *p-value* upper-middle = 0.6251), with a mean Lmax value of 129.5 ± 22.1 10^9 q g^{-1} s^{-1} (**Figure S1**). Similarly, no statistically significant differences were observed in the Lmax values recorded between rachis portions (ANOVA, *p-value* lower-middle = 0.6360; *p-value* lower-upper = 0.4438; *p-value* upper-middle = 0.2548), with a mean Lmax value of 87.9 ± 16.9 10^9 q g^{-1} s^{-1} (**Figure S1**). Finally, the peduncles tested exhibited a significantly lower mean Lmax value (0.6 ± 0.4 10^9 q g^{-1} s^{-1}) compared to the rachis (ANOVA, *p-value* = 0.0298). Comparatively, *F. quadrangularis* luciferase activity presents a mean Lmax value of 313.8 ± 99.2 10^9 q g^{-1} s^{-1}. To complete the data on the sea-pen light emission spectrum, the *in vivo* light emission spectrum of *A. murrayi* was measured and revealed a peak wavelength at 513 nm (**Figure 1G**).

Pennatula phosphorea *maintains its bioluminescence ability after one year in captivity without an exogenous supply of coelenterazine.*

Before the experiment, visual assessments of *P. phosphorea* luminescence were performed in the dark. These observations confirmed that the species maintained the ability to produce visible light even after six–12 months of captivity without any external sources of coelenterazine-containing food.

Measurements of luminescence parameters showed a general decrease in all three parameters for both the pinnules and the rachis (**Figure S2)**. For the pinnules, the maximum light emission shows statistically significant differences upon KCl application (Kruskal-Wallis test, *p-value* = 1.8 10^{-5}), with a mean Ltot value of 361.7 ± 34.6 10^9 q g^{-1} s^{-1} after field collection. This value is statistically different from the mean value observed after six months of captivity (Wilcoxon sum-rank test, *p-value* = 1.5 10^{-6}) but not from the value after 12 months (Wilcoxon sum-rank test, *p-value* = 0.16). The mean Ltot values after 6 and 12 months are 80.5 ± 21.8 and 223.8 ± 84.4 10^9 q g^{-1} s^{-1}, respectively. Coelenterazine content also presented statistically significant differences (Kruskal-Wallis test, *p-value* = 1.3 10^{-5}). The mean coelenterazine content is already drastically reduced after 6 months (30.7 ± 4.5 ng g^{-1}) but remains stable for one year (28.1 ± 4.4 ng g^{-1}) (Wilcoxon sum-rank test, T0 *VS* T6: *p-value* = 0.0001; T0 *VS* T12: *p-value* = 0.0004), without statistical differences between the former two (Wilcoxon sum-rank test, *p-value* = 0.91) (**Figure S2**). Similarly, the luciferase activities decreased over the year and presented statistically significant differences (Kruskal-Wallis test, *p-value* = 0.01). Differences occur between the initial Lmax value (113.2 ± 12.7 10^9 q g^{-1} s^{-1}) and the mean Lmax values of 77.0 ± 16.2 and 43.0 ± 3.7 10^9 q g^{-1} s^{-1} after 6 and 12 months, respectively (Wilcoxon sum-rank test, T0 *VS* T6: *p-value* = 0.383; T0 *VS* T12: *p-value*

500 = 0.013; T6 *VS* T12: *p-value* = 0.383) (**Figure S2**). Similar observations occurred for the three
501 parameters recorded on the rachis portions of *P. phosphorea* (**Figure S2**).
502
503 ***De novo transcriptomes of* Pennatula phosphorea *and* Anthoptilum murrayi**
504
505 For *P. phosphorea*, a total of 47.27 million raw reads of 200 bp length were
506 generated from the pinnule library, 47.27 million from the rachis library, and 41.96 million
507 from the peduncle library. Data quality was assessed using FastQC software. Raw reads are
508 available on the NCBI SRA database: *A. murrayi* (PRJNA1144931), *P. phosphorea*
509 (PRJNA1152785). After low-quality reads filtering, the remaining high-quality reads (*i.e.,*
510 45.29 for the pinnule transcriptome, 45.53 for the rachis transcriptome, and 40.29 for the
511 peduncle transcriptome) were used to assemble a reference transcriptome using the Trinity
512 software. The obtained Trinity-predicted transcripts were clustered using TGICL to obtain
513 the final unigenes.
514 In total, 49,510 unigenes (i.e., non-redundant unique sequences) were obtained with
515 a total length of 72,928,901 bp. The average length was 1,473 bp and the N50 was 2,350 bp.
516 Among the transcriptome data, 35,439 unigenes for the pinnule dataset, 33,778 unigenes for
517 the rachis dataset, and 31,001 unigenes for the peduncle dataset were obtained, with a total
518 of 49,510 different unigenes. The length distributions of the unigenes are shown in **Figure**
519 **2A** and the numerical data are summarized in **Tables S4** and **S5**.
520 Of the 46,258 predicted unigenes, 1,690 were found only in the pinnule
521 transcriptome, 1,114 only in the rachis transcriptome, 1,035 in the peduncle transcriptome,
522 and 36,934 in the peduncle transcriptome. For descriptive purposes, comparative gene
523 expression analysis was performed by mapping FPKM values (*e.g.,* $\log_{10}$(FPKM value pinnule
524 transcriptome) against $\log_{10}$ (FPKM value rachis transcriptome)) calculated for all predicted
525 unigenes (**Table S6**). However, it has to be clarified that transcriptome data have been
526 generated for new gene discovery, not differential expression analyses, as no biological or
527 technical replication was performed as a part of the study. The main species represented
528 within the unigene annotation of the reference transcriptome was the anthozoan
529 *Dendronephthya gigantea* (Verrill, 1864) (79%) (**Figure 2B**). Of the 49,510 *P. phosphorea*
530 unigenes present in the filtered reference transcriptome, 34,984 showed significant matches
531 with the molecular databases: 33,896 to NR (68.5%, E-value < $1e^{-5}$), 8,818 to NT (17.8%),
532 26,473 to SwissProt (53.5%), 28,290 to KEGG (57.1%), 24,642 to KOG (49.8%), 26,790 to
533 InterPro (54.1%), and 13,742 to GO (27.8%) (**Figure 2C**).
534 For *A. murrayi*, 66,425 unigenes were obtained, with a total length of 54,366,500 bp.
535 The average mean length was 818 bp and the N50 was 1140 bp. The length distributions of
536 the unigenes are shown in **Figure 2D** and the numerical data are summarized in **Tables S4**
537 and **S5**. For descriptive purposes, gene expression analysis was performed by mapping the
538 FPKM values (e.g., $\log_{10}$(FPKM value)) calculated for all predicted unigenes (**Table S6**). The
539 main represented species within the unigene annotation of the reference transcriptome was
540 the anthozoan *Paramuricea clavata* (29%) (**Figure 2E**). Among the 66,425 *A. murrayi*

unigenes present in the filtered reference transcriptome, 58,345 were significantly matched to the molecular databases: 41,512 to NR (71.15%, E-value < 1e-10), 11,345 to NT (19.44%), 25,769 to SwissProt (44.16%), 23,549 to KEGG (40.36%), 15,178 to KOG (26.01%), 22,134 to InterPro (37.93%), and 15,178 to GO (26.01%) (**Figure 2F**).

Because of the lack of a reference genome in *P. phosphorea* and *A. murrayi*, and possibly the relatively short length of some unigene sequences, 29.4% and 71.6%, respectively, of the assembled sequences could not be matched to any known genes.

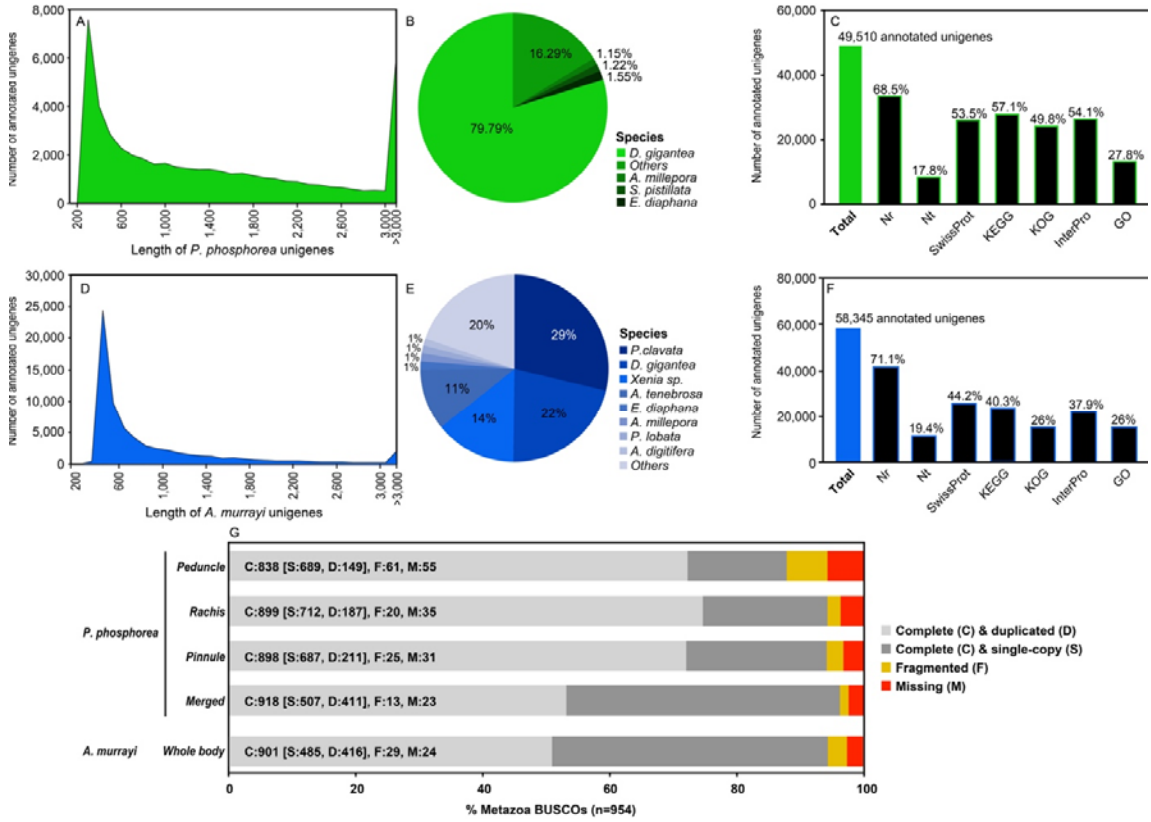

Figure 2. General description of the transcriptomic data. (A) The length distribution of *P. phosphorea* unigenes. (B) Taxonomic annotation of *the P. phosphorea* transcriptome. (C) Global annotation of *P. phosphorea* transcriptome. (D) Length distribution of *the A. murrayi* unigenes. (E) Taxonomic annotation of *A. murrayi* transcriptome. (F) Global annotation of *the A. murrayi* transcriptome. (G) Busco analyses.

Based on Benchmarking Universal Single-Copy Orthologs (BUSCO) analysis, 96.23% of metazoa BUSCO genes were predicted to be complete in the merged *P. phosphorea* transcriptome. In parallel, 1.36% of BUSCO genes were fragmented and 2.41% were missing (**Figure 2G**). Similar results were obtained for *A. murrayi*, with 94.44% complete BUSCO genes found, while 3.04% of BUSCO genes were fragmented, and 2.52% were missing (**Figure 2G**).

Analyses of unigene expression revealed a similar proportion of FPKM values in the three tissues (**Figure 3A, B**). Comparatively, a large number of unigenes appeared to be more highly expressed in the pinnule and rachis than in the peduncle tissue (**Figure 3C**). The

pinnule and rachis tissues appeared to be more similar in terms of the unigene expression profile. The "Molecular function" GO functional annotations for the 40 most expressed unigenes of each sample of *P. phosphorea* (**Figure 3D**) and the whole animal sample for *A. murrayi* (**Figure 3F**) show a classical high expression of molecular actors involved in the cellular machinery and gene regulation. The GO functional annotations for the 40 unigenes with the most pronounced expression differences between tissues, including those highly expressed in one tissue relative to the other and those with lower expression levels, are shown in **Figure 3F**. We did not perform formal differential gene expression analysis, as no replication was performed. Calcium ion binding function (GO: 0005509) appeared to be predominantly expressed in pinnule and rachis tissues, compared to the peduncle (**Figure 3F**). Similarly, the pinnule tissue (containing the feeding polyp) presented a higher proportion of genes annotated as digestive enzymes (**Figure 3F**).

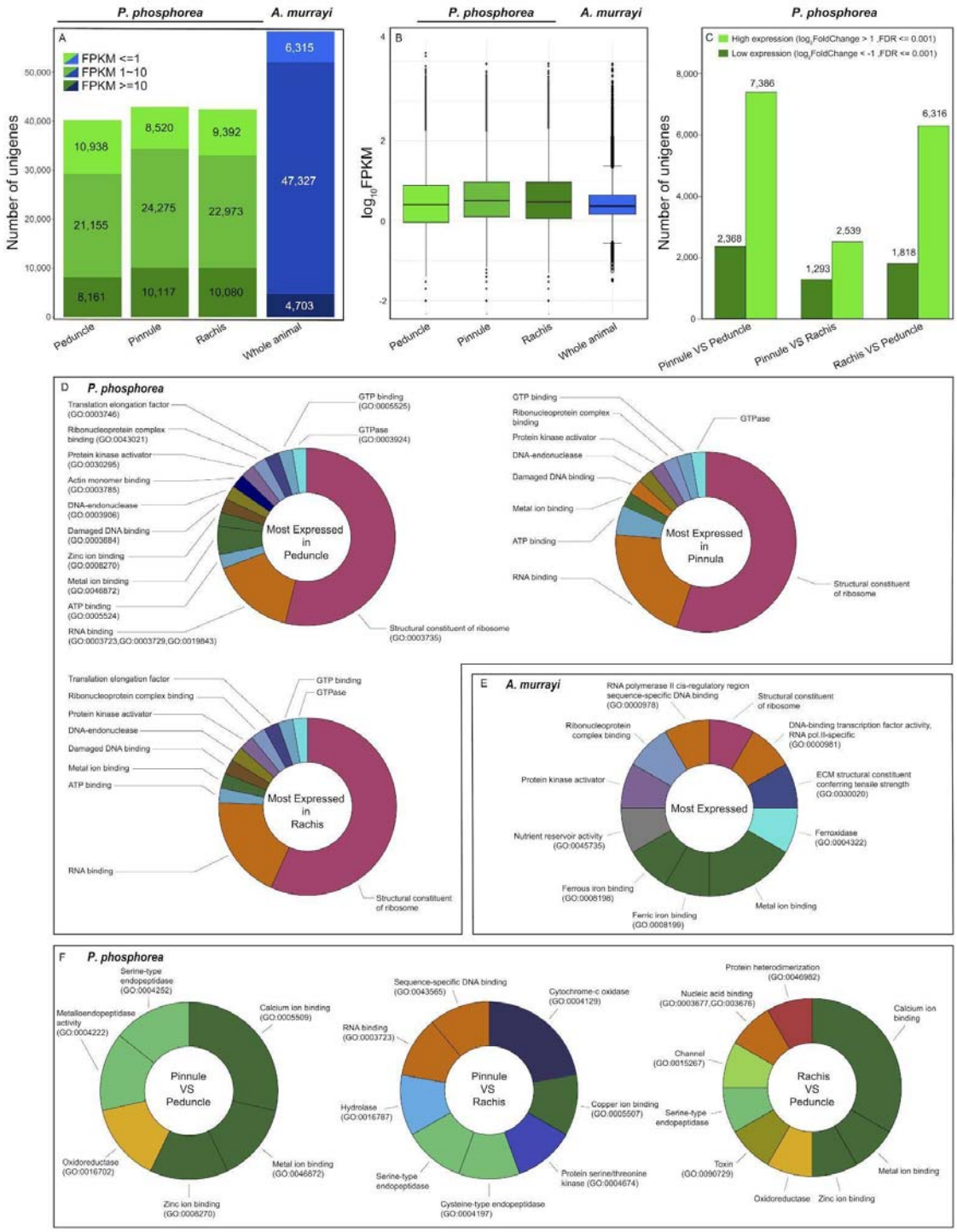

Figure 3. Global gene expression and gene ontology of *Pennatula phosphorea* and *Anthoptilum murrayi* transcriptomic data. (A) Distribution of FPKM expression values across *the P. phosphorea* and *A. murrayi* transcriptomes. (B) Gene expression distribution for each sample. (C) Proportions of unigenes with relatively high or low expression levels in *P. phosphorea* samples. Gene ontology distribution of the 40 most highly expressed unigenes for each sample of *P. phosphorea* (D) and *A. murrayi* (E). (F) Comparison of gene ontology repartition of the 40 most highly expressed unigenes in *P. phosphorea* samples.

585 ***Expression of bioluminescence-related genes in* Pennatula phosphorea *and* Anthoptilum**
586 **murrayi**
587
588 The *P. phosphorea* and *A. murrayi* transcriptomes contained sequences of several
589 predicted luciferases, GFPs, and luciferin-binding proteins. The FPKM values retrieved from
590 each transcriptome are shown in **Table S6**. Reciprocal BLAST analyses revealed that the
591 sequences matched the luciferases, CBPs, and GFPs of Anthozoans.
592 Several *R*Luc-like enzymes were recovered from both investigated species (*A. murrayi*
593 and *P. phosphorea*). In addition, sequence mining allowed us to recover additional *R*Luc-like
594 sequences from the genomes of *Renilla muelleri* and *R. reniformis*. Phylogenetic analyses
595 revealed three clades of *R*Luc-like enzymes in Pennatulacea (**Figure 4A**). Clade A contains
596 well-known luciferases from *R. muelleri* and *R. reniformis* and probable luciferase sequences
597 from *A. murrayi*, *P. phosphorea,* and *Cavernularia obesa* (Valenciennes, 1850). Interestingly,
598 clade A did not contain any sequences from the non-luminous species. Clade B, in
599 comparison, includes several sequences from non-luminous species (*e.g., Pinnigorgia flava*
600 (Nutting, 1910) and *Sinularia cruciata* (Tixier-Durivault, 1970)), in addition to several
601 sequences from both our model species. Clade C also contained *the R*Luc-like enzymes
602 retrieved from each transcriptome.

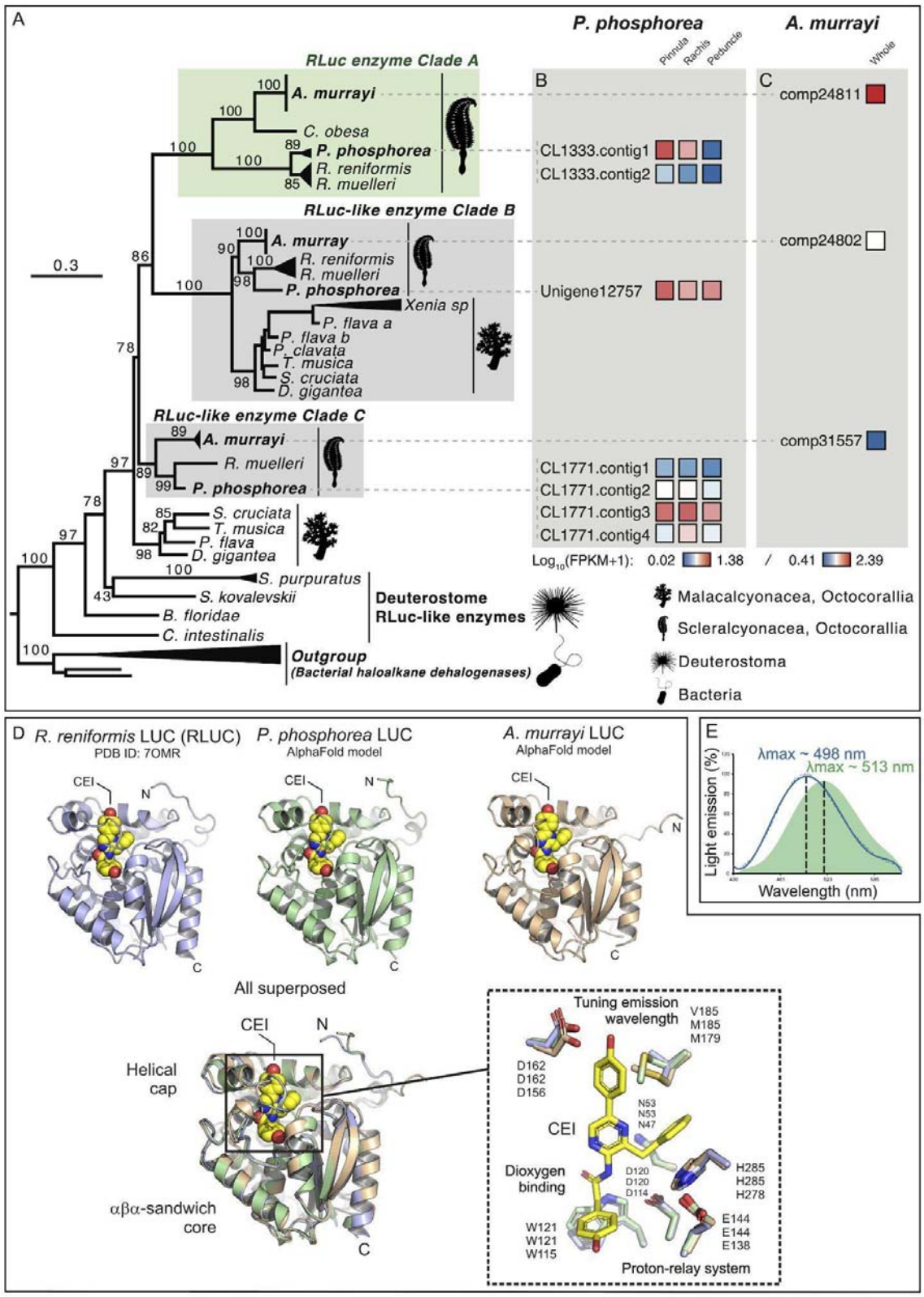

Figure 4. Phylogenetic tree of *R*Luc-like enzymes, including *P. phosphorea* and *A. murrayi* amino acid sequences. (A) Maximum likelihood tree based on the amino acid sequence alignment of *R*Luc-like enzymes. The tree was calculated by the IQ-tree software using the LG+I+G4 model of evolution. Numbers at the nodes indicate ultrafast bootstrap values based on 1000 replicates. The scale bar represents the percentage of amino

608 acid substitutions per site. Bacterial haloalkane dehalogenase sequences were used to root the tree. (B) The
609 expression level of each retrieved *R*Luc-like sequence in a distinct portion of *P. phosphorea*. (C) Expression level
610 of each retrieved *R*Luc-like sequence in *the whole A. murrayi* specimen. (D) Structural comparison of AlphaFold
611 models of *P. phosphorea* and *A. murrayi* Luc proteins and the crystal structure of *R. reniformis* Luc complexes
612 with coelenteramide (CEI) oxyluciferin (PDB ID: 7OMR). (E) Superimposed spectrum of the *in vivo* luminescence
613 of *A. murrayi* (green) and the *in vitro* luminescent assay of *A. murrayi* luciferase in the presence of
614 coelenterazine (fc.: 6 µM) (blue).

615 The retrieved sequence (CL1333; **Figure 4B**) of *P. phosphorea* luciferase has an
616 estimated molecular weight of 35.84 kDa. A comparison of the amino acid sequences of *P.*
617 *phosphorea* and anthozoan luciferases demonstrated the presence of the catalytic triad
618 involved in luciferase activity (**Figure S3; File S1**). These key sites consist of an aspartate
619 residue in position 120, a glutamate residue in position 144, and a histidine in position 285.
620 Residues asparagine 53 and tryptophan 121 (N53 and W121), previously established for the
621 O_2 stabilization and the CO_2 release within *Renilla* luciferase [14], were also retrieved in our
622 luciferase sequences (**Figure S3**). The retrieved *P. phosphorea* luciferase sequence, based on
623 RNA-seq data, appears to be highly similar to other known anthozoan luciferases. It shares
624 90.26% identity and 95% similarity with *Renilla reniformis* luciferase (*Renilla*-luciferin 2-
625 monooxygenase). This sequence was validated by DNA amplification and sequencing using
626 *R*Luc primers. FPKM analyses revealed that this sequence was mostly expressed in the
627 pinnule and rachis (**Figure 4B**).

628 The *A. murrayi* luciferase (Comp24811, **Figure 4C**), with a molecular weight estimated
629 at 34.61 kDa and consisting of 304 amino acids, exhibits 58% sequence identity and 98%
630 coverage compared to *R*Luc, highlighting significant similarities. Sequence alignment of *A.*
631 *murrayi* luciferase with *R*Luc has revealed the conservation of the catalytic triad and active
632 site. The *R*Luc structure features two distinct domains: a cap domain and alpha/beta-
633 hydrolase domain. Key residues essential for enzymatic activity, including the substrate
634 entry tunnel and catalytic triad (D120, E144, and H285), are located in the cap domain
635 (**Figure S3**). These elements have also been identified in the luciferase sequence of *A.*
636 *murrayi*, as reported by Rahnama et al., 2017 [62] and Khoshnevisan et al. 2018 [63] for
637 *Renilla* luciferase. Through the expression of recombinant luciferase in *Escherichia coli* using
638 degenerate primers derived from *A. murrayi* transcriptome analysis, *A. murrayi* luciferase
639 was tested for preliminary downstream expression, yielding an active enzyme capable of
640 producing blue light (λmax = 498 nm) upon coelenterazine addition (**Figure 4E**).

641 Structural models of *P. phosphorea* and *A. murrayi* LUCs show a canonical aba-
642 sandwich fold with a helical cap domain (**Figure 4D**). Overall comparison between the crystal
643 structure of *R. reniformis* LUC complexed with coelenteramide (CEI) oxyluciferin and
644 structural models of *P. phosphorea* and *A. murrayi* LUCs showed root-mean-square deviation
645 (RMSD) on the C_a-atoms of 0.7 and 1.3, respectively. Careful inspection of the modeled LUC
646 structures revealed that key residues of the catalytic pentad are conserved and properly
647 positioned for productive catalysis (**Figure 4D**). From these, three residues (aspartate-

histidine-glutamate) function as a protein-relay system protonating a CEI oxyluciferin at an amide nitrogen, while the two residues (asparagine and tryptophan) are responsible for co-substrate (dioxygen) binding. Moreover, an aspartate residue, responsible for tuning the emission wavelength, found on the rim of the catalytic pocket in *R. reniformis* luciferase [14], is also conserved in these luminescent species.

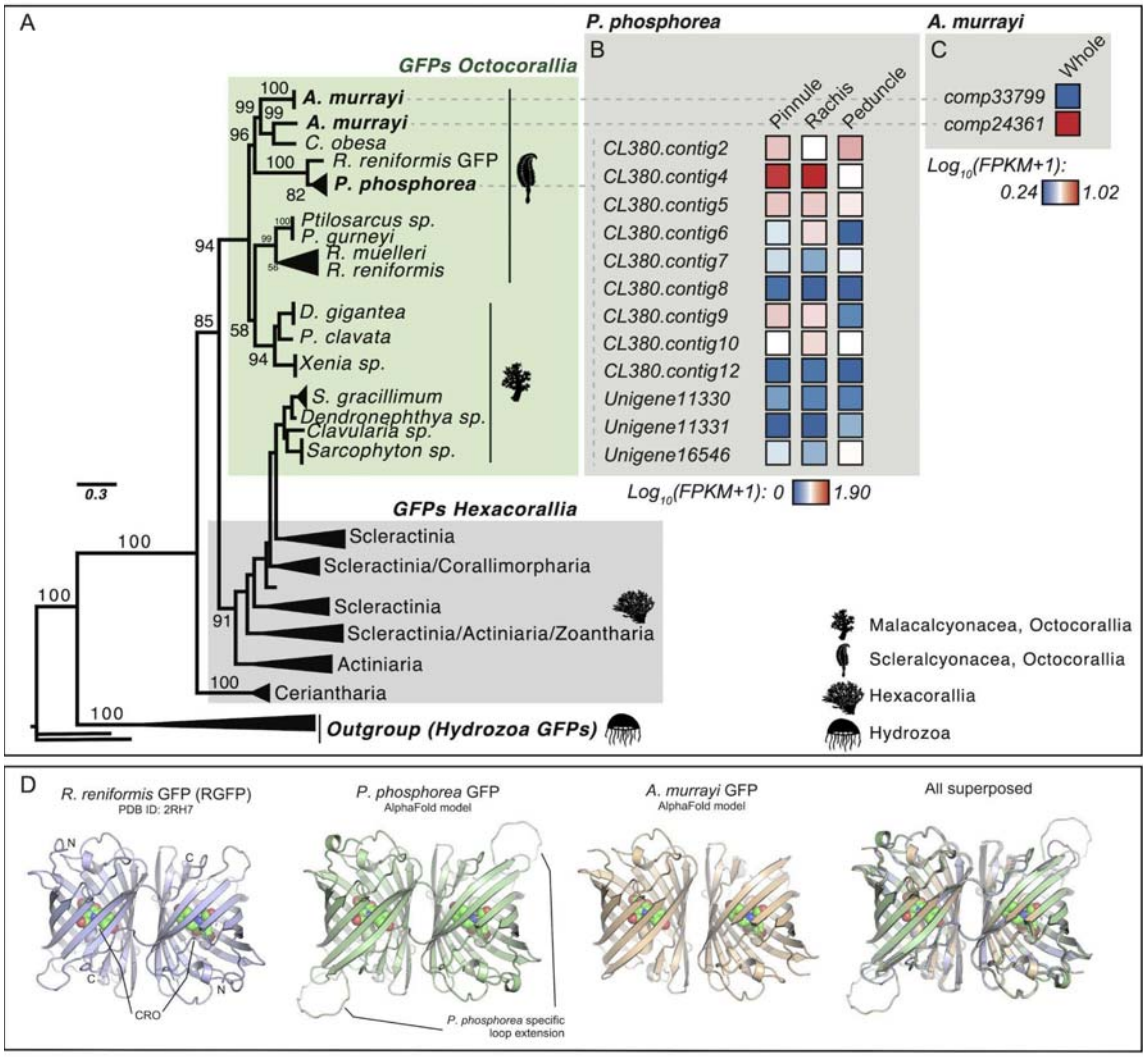

Figure 5. Phylogenetic tree of anthozoan fluorescent proteins, including *P. phosphorea* and *A. murrayi* amino acid sequences. (A) Maximum likelihood tree based on green fluorescent protein amino acid sequence alignment. The tree was calculated by the IQ-tree software using the WAG+R4 model of evolution. Numbers at the nodes indicate ultrafast bootstrap percentages based on 1,000 replicates. The scale bar represents the percentage of amino acid substitutions per site. Hydrozoan GFP sequences were used to root the tree. (B) The expression level of each retrieved GFP sequence for a distinct portion of *P. phosphorea*. (C) The expression level of each retrieved GFP sequence in *the whole A. murrayi* specimen. (D) Structural comparison of AlphaFold models of *P. phosphorea* and *A. murrayi* GFP proteins and the crystal structure of *R. reniformis* GFP (PDB ID: 2HR7).

Several sequences coding for GFP-like sequences were retrieved from *the P. phosphorea* and *A. murrayi* transcriptomes. *P. phosphorea* GFP (CL380; 20.81 kDa) and *A. murrayi* GFP

666 (Comp24361; 27.24 kDa) appear homologous to other anthozoan sequences, and both
667 sequences clustered with GFP sequences of bioluminescent Scleralcyonacea (**Figure 5A;**
668 **Figure S3; File S2**). *P. phosphorea* GFP shares 79.42% identity and 86% similarity with the
669 GFP of *R. reniformis*. In comparison, *A. murrayi* GFP shared 73.06% identity and 87%
670 similarity with the GFP of *Cavernularia obesa*. Pinnules and rachises were the main sites of *P.*
671 *phosphorea* GFP expression (**Figure 5B**). Interestingly, a perfect sequence repetition was
672 observed in the most expressed *P. phosphorea* GFP sequence (**Figure S3**). Among the
673 unigene pairs found in the *A. murrayi* transcriptome, Comp24361 appeared to be more
674 highly expressed (**Figure 5C**). Sequence analysis pinpointed a lack of N-terminal part for the
675 *Anthoptilum* sequence (**Figure S3**).
676 Structural models of *P. phosphorea* and *A. murrayi* GFPs show a characteristic β-
677 barrel fold with a fluorophore moiety (CRO) covalently bound inside the barrel (**Figure 5D**).
678 *In silico* modeling suggests that these proteins may associate as homodimers, similar to the
679 homodimeric structure observed in the crystal structure of *R. reniformis* GFP. However,
680 further experimental validation is required to confirm this hypothesis. Comparison between
681 the crystal structure of *R. reniformis* GFP and models of *P. phosphorea* and *A. murrayi* GFPs
682 showed RMSD on the C_a-atoms of 0.9 and 1.1, respectively, highlighting their high
683 similarities. A structural feature distinguishing *P. phosphorea* and *A. murrayi* GFPs from their
684 *R. reniformis* counterpart is the composition of the fluorophore moiety. While *R. reniformis*
685 fluorophore is generated from a serine-tyrosine-glycine tripeptide, the fluorophores of *P.*
686 *phosphorea* and *A. murrayi* are formed from a glutamine-tyrosine-glycine tripeptide, which
687 may affect the fluorescent properties of these proteins. Moreover, there is one markedly
688 extended solvent-exposed loop in *P. phosphorea* GFP (**Figure 5D**). We believe that this
689 species-specific extension might affect protein–protein complexation during the
690 radiationless resonance energy transfer process, but future experimental evidence is needed
691 to verify this hypothesis.
692

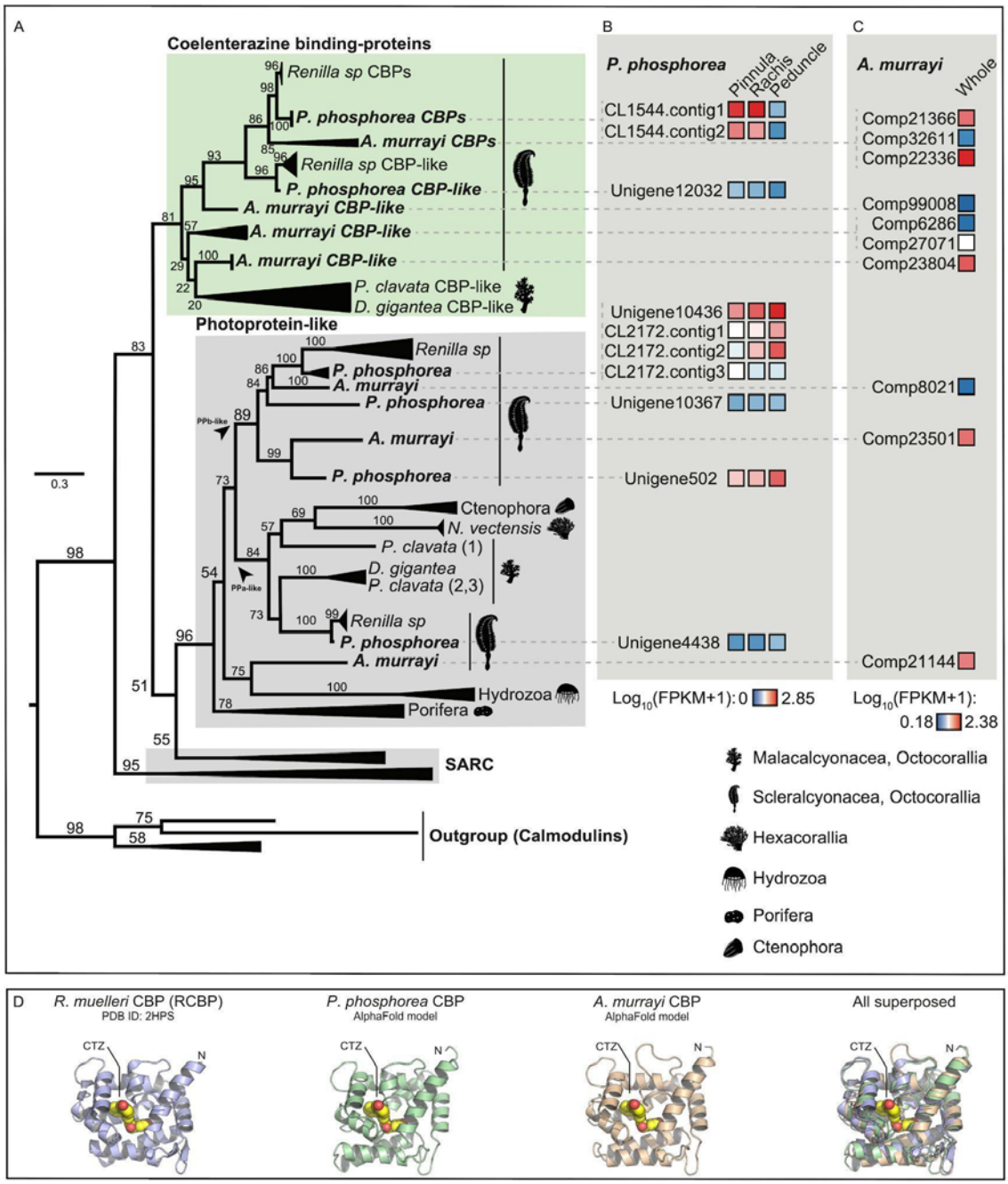

Figure 6. Phylogenetic tree of coelenterazine-binding proteins, including *P. phosphorea* and *A. murrayi* amino acid sequences. (A) Maximum likelihood tree based on the amino acid sequence alignment of coelenterazine-binding proteins. The tree was calculated by the IQ-tree software using the LG+R4 model of evolution. Numbers at the nodes indicate ultrafast bootstrap percentages based on 1000 replicates. The scale bar represents the percentage of amino acid substitutions per site. Calmodulin sequences were used to root the tree. (B) The expression level of each retrieved CBP and CBP-like sequence for a distinct portion of *P. phosphorea*. (C) Expression level of each retrieved CBP and CBP-like sequence in *the whole A. murrayi* specimen. (D) Structural comparison of AlphaFold models of *P. phosphorea* and *A. murrayi* CBP proteins and the crystal structure of *R. muelleri* CBP complexes with coelenterazine (CTZ) luciferin (PDB ID: 2HPS).

704 Different sequences of CBPs and CBPs-like were retrieved from *the transcriptomes of*
705 *P. phosphorea and A. murrayi*. Some of these sequences clustered with the CBPs of luminous
706 Scleralcyonacea, whereas others were found to be clustered with photoprotein-like proteins
707 (**Figure 6A; File S3**). One sequence appeared to be mainly expressed within the *P.*
708 *phosphorea* pinnule and rachis (CL1544; 26.84 kDa) and *the A. murrayi* colony (Comp 22336;
709 21.08 kDa) (**Figure 6B, C**). The most highly expressed *P. phosphorea* CBP appeared highly
710 similar to other luminous anthozoan sequences. *P. phosphorea* CBP shared 85.33% identity
711 and 94% similarity with the luciferin-binding protein of *R. reniformis*, while *A. murrayi* CBP
712 shared 50% identity and 74% similarity with the luciferin-binding of *R. reniformis*.
713 Interestingly, sequences clustered in the photoprotein-like protein group appeared to be
714 mainly expressed within the non-photogenic peduncle tissue in *P. phosphorea*.
715 Finally, structural models of *P. phosphorea* and *A. murrayi* Ca^{2+}-regulated CBPs reveal
716 a typical EF-hand fold, containing three Ca^{2+}-binding sites. As shown in **Figure 6D**,
717 comparison between the crystal structure of *R. reniformis* CBP complexed with
718 coelenterazine (CTZ) luciferin and structural models of *P. phosphorea* and *A. murrayi* LUCs
719 show a structural similarity, with RMSD on the C_a-atoms of 2.3 and 3.2, respectively. The
720 RMSD values were higher than those observed for LUC and GFP proteins, but this is likely
721 caused by a large conformational space that is searched by CBP proteins. Importantly, our
722 modeling reveals an internal cavity in *P. phosphorea* and *A. murrayi* CBPs that is capable of
723 accommodating CTZ luciferin, suggesting that these proteins are indeed functional luciferin-
724 binding proteins (**Figure 6D**).
725
726 ***Luciferase expression and green autofluorescence in* Pennatula phosphorea *and* Funiculina**
727 **quadrangularis**
728
729 Based on the high sequence similarity of *P. phosphorea* luciferase with *Renilla*
730 luciferase, a commercial anti-Renilla luciferase antibody was selected for immunodetection.
731 Immunoblot analyses revealed strong anti-luciferase immunoreactive bands in both extracts
732 of the pinnule and rachis tissues (**Figure S4**). The bands correspond to a protein with an
733 approximate molecular weight of 35 kDa, matching the molecular weight of the predicted *P.*
734 *phosphorea* luciferase and the *Renilla* luciferase molecular weight of 36 kDa. No labeling was
735 detected in the peduncle tissue extract (**Figure S4**).
736 On autozooid polyps of the pinnules (**Figure 7A-D**), a strong green autofluorescent
737 signal was observed at the tentacle crown base before (**Figure 7B**) and after (**Figure 7C**)
738 paraformaldehyde fixation. This fluorescent signal is located in clusters of cells at the
739 tentacle junctions. Strong anti-*Renilla* luciferase immunoreactivity was observed at the same
740 level as the green fluorescence signal (**Figure 7C, D**). On siphonozooid polyps of the rachis,
741 the autofluorescent signal was also observable and was located as green dots (from 10 to 25
742 µm diameter) spread in the tissue, generally in pairs (**Figure 7E**). Anti-*Renilla* luciferase-
743 positive cells colocalized with these autofluorescent dots (**Figure 7E, F**). Finally, no green
744 fluorescence or immunolabeling was detected in peduncle tissue (data not shown).

For *Funiculina* polyps (**Figure 7G**), a green autofluorescent signal was observed in the freshly dissected specimens before fixation (**Figure 7H**). This green autofluorescence completely disappeared after fixation (**Figure 7I**). Luciferase localization differed from that in *P. phosphorea*. A strong luciferase signal was detected within the polyp tentacle tissue and not at the base of the polyp crown (**Figure 7I, J**).

Negative controls with the omission of the primary antibody did not reveal any non-specific binding of the secondary antibodies (data not shown).

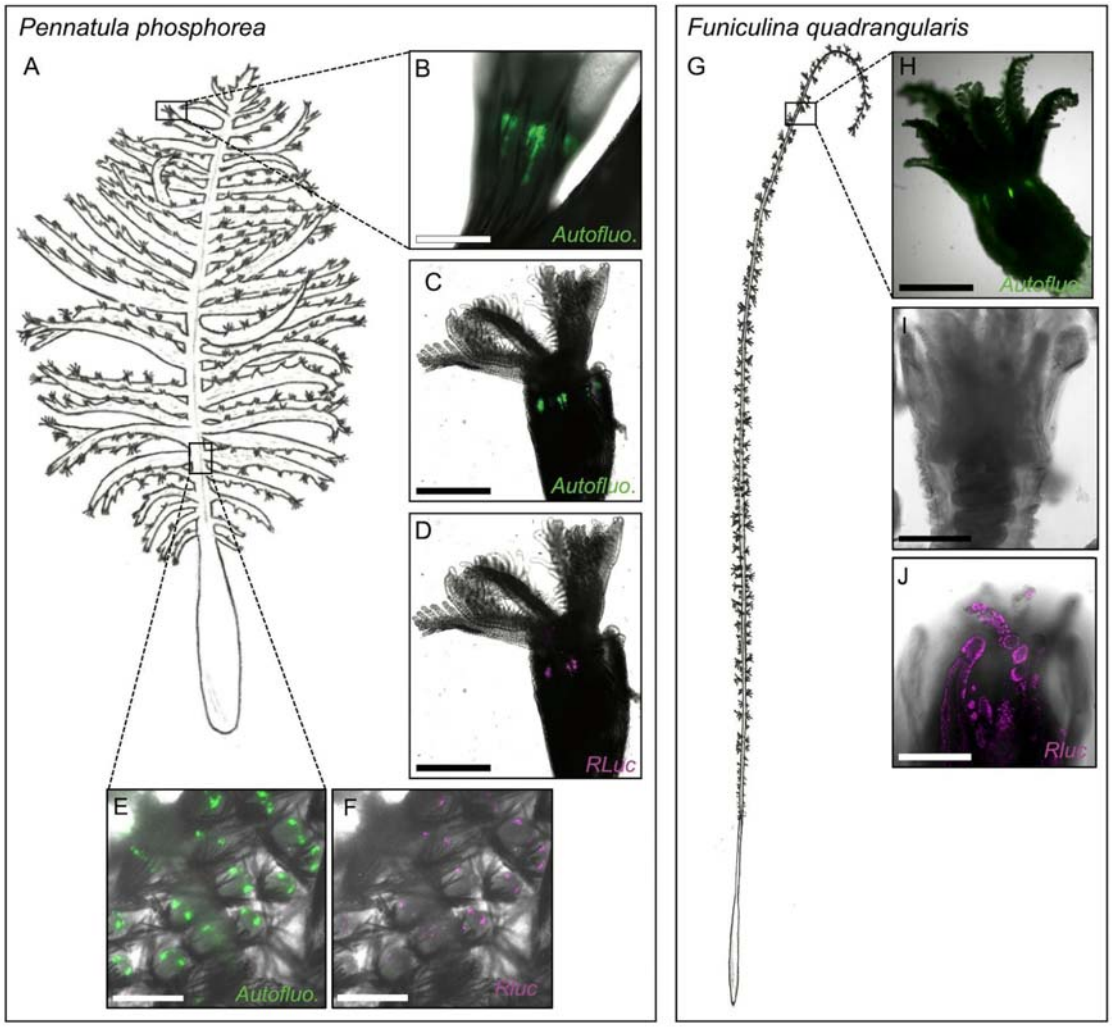

Figure 7. Autofluorescence and luciferase immunodetection in *P. phosphorea* and *F. quadrangularis*. (A) Schematic illustration of *P. phosphorea*. Natural green autofluorescence (B), green fluorescence after fixation (C), and luciferase immunodetection (D; magenta) of the *P. phosphorea* pinnule autozooids. Green fluorescence after fixation (E) and luciferase immunodetection (F; magenta) in *P. phosphorea* rachis siphonozooids. (G) Schematic illustration of *F. quadrangularis*. Natural green autofluorescence (H), observation after fixation with no autofluorescent signal (I), and luciferase immunodetection (J; magenta) of *the F. quadrangularis* autozooids. Scales: B-F, H - 500 µm; I, J - 250 µm.

***Calcium is involved in the bioluminescence of* Pennatula phosphorea *and* Funiculina quadrangularis**

763
764 Based on *P. phosphorea* coelenterazine-binding protein retrieval in the *Pennatula*
765 transcriptome data and the literature mentioning the potential implication of Ca^{2+} in the
766 release of luciferin from coelenterazine-binding proteins, Ca^{2+} involvement in the light
767 emission process of *P. phosphorea* and *F. quadrangularis* was investigated. The tested
768 specimens of both species revealed a drastic increase in light production when immersed in
769 ASW with a doubled Ca^{2+} ion concentration (20 mM) (**Figure 8A, B**). At the same time, no
770 statistical differences were observed between the normal ASW (10 mM) and ASW devoted
771 to Ca^{2+} ions (0 mM) (**Figure 8A, B**). Analysis of the effects of the A23187 ionophore showed
772 no statistical differences compared to the calcium concentration (**Figure 8C, D**). For both
773 specimens, adrenaline triggered light production when calcium was present in ASW (**Figure**
774 **8E, F**). While an increase in the mean Ltot was observed between adrenaline tested samples
775 at 10 mM and 20 mM of $CaCl_2$ in the medium, this increase was not statistically supported
776 (**Figure 8E, F**). Finally, no significant differences were observed in Ltot after KCl application at
777 the three Ca^{2+} concentrations (**Figure S5**).
778

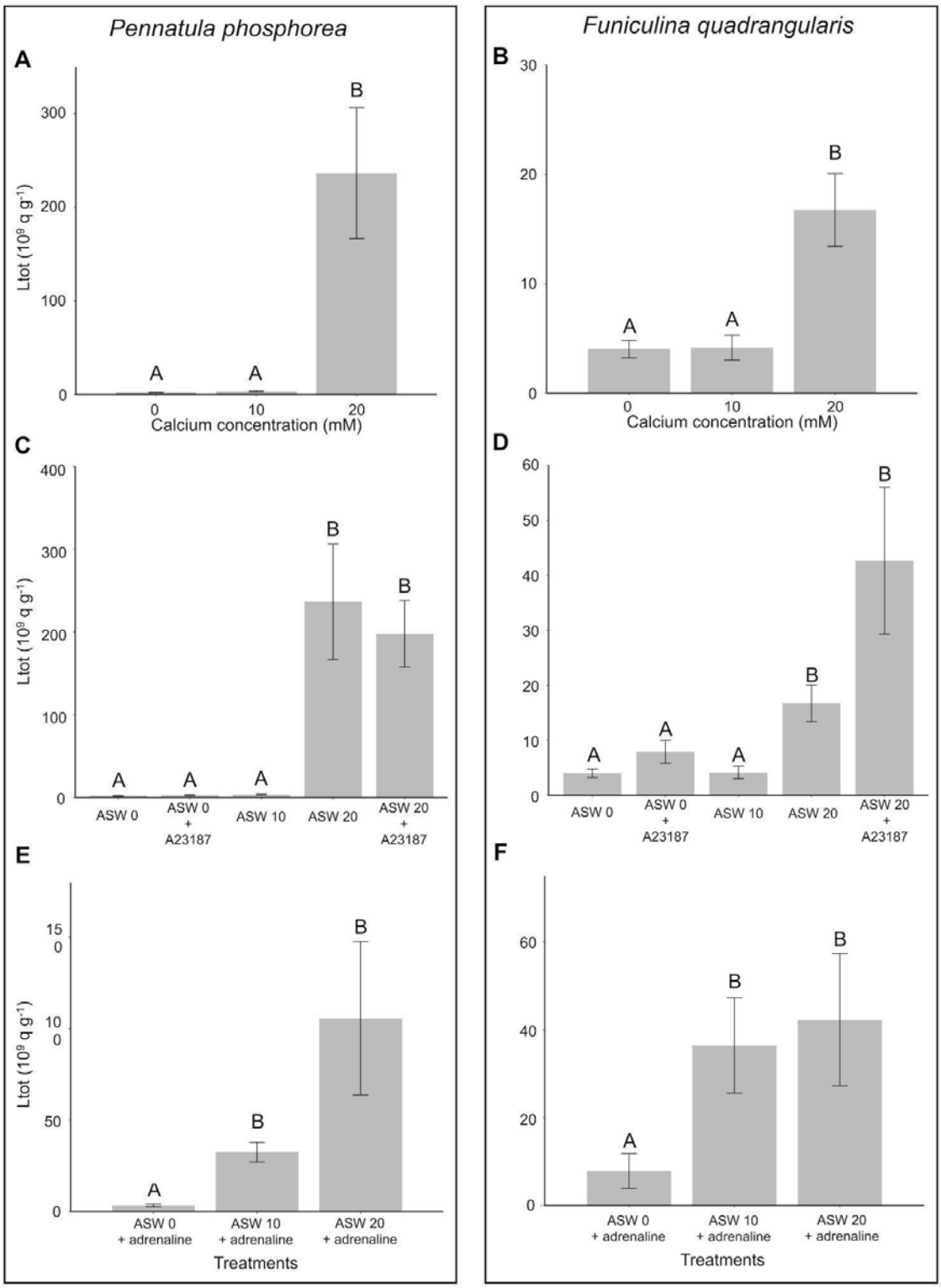

Figure 8. Calcium involvement in *P. phosphorea* and *F. quadrangularis* light emissions. Experiments were performed on *P. phosphorea* (A, C, E) and *F. quadrangularis* (B, D, F). Effect of different concentrations of calcium (0, 10, 20 mM) in the medium on the total light emission (Ltot) (A, B). Effect of different calcium concentrations (0, 10, 20 mM) in the medium in the presence and absence of the calcium ionophore A23187 on the Ltot (C, D). Effect of different concentrations of calcium (0, 10, 20 mM) in the medium in the presence of adrenaline (10^{-5} mol L^{-1}) on the Ltot (E, F). different lettering indicates statistical differences.

786
787 **Discussion**
788
789 Through biochemical cross-reaction experiments, this study demonstrated that the
790 bioluminescence of *P. phosphorea*, *F. quadrangularis*, and *A. murrayi* is associated with a
791 coelenterazine-dependent luciferase homologous to the well-known luciferase of the sea
792 pansy *Renilla*. The measured concentration of coelenterazine in *P. phosphorea* pinnules
793 closely aligns with the reported values of 141 and 282.4 ng g^{-1} for the phylogenetically
794 closely related species *R. muelleri* and *C. obesa*, respectively [1]. Similarly, the mean
795 luciferase activity of *P. phosphorea* pinnules reaches a comparable range as other organisms
796 using *Renilla*-type luciferases such as *R. muelleri* (± 130 10^9 q g^{-1} s^{-1}) and *C. obesa* (± 220 10^9 q
797 g^{-1} s^{-1}), or the sympatric ophiuroid *Amphiura filiformis* (± 69 10^9 q g^{-1} s^{-1}) [1,64]. While the
798 luciferase activity recorded for *F. quadrangularis* is higher than *P. phosphorea*, this species
799 exhibits a smaller coelenterazine content, being closer to recorded values of the
800 echinoderms *A. filiformis* (5.4 ng g^{-1}; [64]) or the crinoid *Thalassometra gracilis* (Carpenter,
801 1888) (4.5 ng g^{-1}; [65]). Transcriptome and phylogenetic analyses confirm results for *P.*
802 *phosphorea* and *A. murrayi* with a clear sequence conservation of the retrieved luciferases
803 with the *Renilla* luciferase. Consistent with the literature, species such as *D. gracile* or
804 undetermined species from the genera *Umbellula*, *Pennatula*, and *Funiculina* also present
805 evidence of the use of coelenterazine as substrate and a *Renilla*-like luciferase as enzyme of
806 their bioluminescent systems [13].
807 Our phylogenetic analysis underlines three distinctive clades of *Renilla*-like luciferase.
808 One of these clades (Clade A) contains all the known sequences of anthozoan light-emitting
809 luciferases. The other two clades (Clades B and C) contain other homologous *R*luc-like
810 sequences, notably from non-luminous species. The related biochemical functionality and
811 bioactivity of these B and C clades sequences are unknown and need further investigations
812 to fully apprehend the evolution of luciferase among anthozoans. Nevertheless, this
813 clustering led to hypothesized duplications of the ancestral gene with either (*i*) a neo
814 functionality as a "real" functional luciferase able to catalyze a bioluminescent reaction or (*ii*)
815 a bi-functionality of these enzymes as light-producing enzyme and another ancestrally
816 conserved enzymatic function. The ancestral functionality of the *R*Luc enzyme has been
817 assumed to originate from bacterial haloalkane dehalogenases, enzymes with a hydrolase
818 activity cleaving bonds in halogenated compounds [66]. A basal gene transfer from bacteria
819 until metazoans has been hypothesized [18,66]. Interestingly, *R*Luc-like luciferases have
820 been demonstrated to be the enzymes involved in the bioluminescence of phylogenetically
821 distinct species such as the brittle star *A. filiformis* [18] and the tunicate *P. atlanticum*
822 (Péron, 1804) [19], letting assumed that the sequence was convergently coopted multiple
823 times during the evolution. Consistent with previous research on *R*Luc sequences, our
824 retrieved *P. phosphorea* and *A. murrayi* luciferase (Clade A) present high sequence similarity
825 with the other pennatulaceans functional luciferases, also revealing conservation of the
826 catalytic triads essential for the luciferase catalytic activity [14,51,67]. The complete

827 characterization of *P. phosphorea*, *A. murrayi*, and *F. quadrangularis* luciferases will allow us
828 to better apprehend the functionality and evolution of these luciferase enzymes. Future
829 research will enable us to better characterise these luciferases and also the interactions
830 between these enzymes and their substrates and associated molecules, as is the case with
831 the approach to the role of *Renilla* luciferase residues (e.g., mutagenesis, QM/MM
832 [14,51,67]).
833 While the retrieved GFP sequences are unique and well clustered with other
834 Scleralcyonacea sequences, a similar observation, as for the luciferases, occurs for the CBPs
835 and CBPs-like with multiple retrieved sequences clustered in different groups. The first
836 group represents the functional coelenterazine-binding protein retrieved and characterized
837 in luminous species, while the second group, named photoprotein-like proteins, raise
838 questions on the exact functionality of these retrieved sequences. These photoprotein-like
839 proteins might also be involved in calcium binding. Active photoproteins of cnidarians and
840 ctenophores depend on calcium to trigger light emission [68-71]. Nevertheless, the higher
841 expression within the *P. phosphorea* peduncle assumed another function without a
842 relationship with the bioluminescence.
843 AlphaFold is a neural network machine learning tool for predicting macromolecular
844 structures and complexes, providing structural models with near-atomic accuracy even in
845 the absence of known similar structures [72,73]. Here, we employed AlphaFold to predict
846 macromolecular structures of the most expressed genes encoding for LUC, GFP, and CBP
847 proteins in *P. phosphorea* and *A. murrayi*. Computational predictions yielded structural
848 models with very high confidence scores (>90) for all analyzed proteins and that are
849 structurally similar to crystallographic structures of well-characterized LUC [14], GFP [12],
850 and CBP [74] proteins encoded by the sea pansies *R. reniformis* and *R. muelleri*. Taken
851 together, our structural predictions suggest that the identified *P. phosphorea* and *A. murrayi*
852 LUC, GFP, and CBP proteins with the highest expression values are structurally and
853 functionally relevant and responsible for bioluminescence in these species.
854 Kept in captivity without exogenous coelenterazine supply, *P. phosphorea* can still
855 produce light after one year, even if the coelenterazine content and luciferase activity
856 decrease. Therefore, these results support a *de novo* synthesis of the coelenterazine
857 substrate in *P. phosphorea*. Coelenterazine *de novo* synthesis by luminous marine organisms
858 has been documented for the calanoid copepods *Metridia longa* (Lubbock, 1854) and *M.*
859 *pacifica* (Brodsky, 1950), the oplophorid shrimp, *Systellaspis debilis* (Milne-Edwards, 1881),
860 and two ctenophores, *Mnemiopsis leidyi* (Agassiz, 1865) and *Bolinopsis infundibulum*
861 (Müller, 1776) [75-78]. The natural precursors of coelenterazine have been demonstrated to
862 be the L-tyrosine and L-phenylalanine amino acids in *M. pacifica* [77]. By screening the
863 transcriptomic data of 24 ctenophores, Francis et al., 2015, assumed the involvement of a
864 non-heme iron oxidase-like enzyme, similar to isopenicillin-N-synthase, in the biosynthesis
865 pathway of this luciferin [79]. Future research could be carried out to validate the *de novo*
866 biosynthesis of the coelenterazine bioluminescent substrate, in particular by maintaining *P.*
867 *phosphorea* and their offspring over generations in captivity in the same conditions without

868 coelenterazine supply [78,80]. This protocol could be applied to other pennatulaceans to
869 determine whether the coelenterazine genesis is a common trait in this clade. Nevertheless,
870 the first challenge would be to control the life cycle of these species in captivity. Similarly, it
871 would be interesting to analyze different pennatulacean transcriptomes searching for
872 enzymes homologous to the isopenicillin-N-synthase potentially involved in the
873 coelenterazine biosynthetic pathway, as retrieved in ctenophores.

874 In *P. phosphorea*, the morphological localization of luciferase expression matched the
875 green fluorescent sites obtained in unfixed and fixed tissues. Green autofluorescence
876 observed on unfixed specimens is assumed to be a mix of the native autofluorescence of
877 coelenterazine and the autofluorescent reaction occurring through the GFP, while green
878 autofluorescence observed after tissue fixation corresponds only to the GFP signals.
879 Comparatively, the *in vivo* green fluorescence observed in the *F. quadrangularis* tissues,
880 which disappeared after fixation, was assumed to be related only to the natural
881 autofluorescence of coelenterazine and the lack of GFP in this species. In contrast to *P.*
882 *phosphorea,* which emits green waves of light at λmax = 510 nm, *F. quadrangularis* emits
883 blue at λmax = 485 nm, supporting the absence of GFP for this species [13,36,61,81]. This
884 natural autofluorescence has recently been demonstrated to appear and disappear from the
885 photogenic site, depending on the substrate dietary acquisition of the brittle star *A.*
886 *filiformis*. This species depends on the trophic acquisition of the coelenterazine substrate to
887 produce light [64,82]. When the brittle star was fed with coelenterazine-containing food,
888 green autofluorescent spots appeared at the level of spine-associated photocytes [82]. As
889 for *F. quadrangularis*, a similar disappearance of the green fluorescent signal (possibly
890 attributed to the coelenterazine) has been observed in the fixed tissue of the brittle star
891 species [82]. The autofluorescent sites observed along the tentacle bases of the autozooids
892 of *P. phosphorea* are consistent with the already described location of the autofluorescent
893 photogenic cell processes in autozooids of *Stylatula elongata* [83], and to a lesser extent,
894 *Acanthoptilum gracile,* and *Renilla koellikeri* [83,33]. For the former species, it was noticed
895 that the photocytes process followed the same orientation as the longitudinal muscles,
896 allowing autozooids to retract [33]. On the other hand, the luciferase expression site in *F.*
897 *quadrangularis*, in the cellular processes of the apical part of the tentacle, was never
898 reported before. This location along the polyp tentacles matches the described position of
899 photocytes in autozooids of *Ptilosarcus* species [83].

900 Our spectrum measurement performed with the *A. murrayi* recombinant luciferase is
901 consistent with already observed coelenterazine-dependent systems in other species
902 emitting in the same range of wavelengths. Recorded spectrum for coelenterazine-
903 dependent luciferase systems can vary between 475 to 493 nm in *P. atlanticum*, 482 nm
904 emitted by *R*Luc, 472 nm emitted by the brittle star *A. filiformis*, 455 nm emitted by
905 *Oplophorus gracilirostris* and 485 nm emitted by *F. quadrangularis* [18,19,66,84]. According
906 to the natural spectrum recorded on the whole specimens (λmax = 513 nm), similar to the
907 spectrum measured for *P. phosphorea* [61], and the transcriptomic presence of a GFP
908 sequence in *A. murrayi*, this species is strongly assumed to display a GFP-associated

coelenterazine-dependent luminous system. At least six anthozoan species present expression of a GFP and the production of green light. Some of these species may live in sympatry with anthozoan blue emitters, such as *P. phosphorea* and *F. quadrangularis,* with an overlap of depth repartition and habitat preferences occurring. Therefore, questions arise concerning luminescence's exact function(s) among anthozoans. Even if some assumptions are proposed in the literature, no one has ever developed an ethological protocol to validate them [37]. Therefore, why some anthozoan evolved green light emission while the primary coelenterazine-luciferase reaction produces blue light remains. Different function(s) in the same environment may have led to the acquisition or the loss of the GFP gene by some anthozoan species upon evolutionary constraints.

As demonstrated for other pennatulacean species, CBP seems to be an essential component of the luminous system [21-25,27]. The retrieved CBPs in *P. phosphorea* and *A. murrayi* are congruent with this literature. Gene ontology distribution analyses performed on the different tissues of *P. phosphorea* underline a high expression of calcium ion binding proteins, including the retrieved CL1333 CBP, in the photogenic tissue (pinnule and rachis) of this species. The expression of this gene within the photogenic tissues supports its involvement in the luminous reaction. As demonstrated for *Renilla* by Stepanyuk et al., 2008, CBPs need calcium as a cofactor to release the coelenterazine [29]. In addition to the retrieved CBPs sequence in the *Pennatula* transcriptome, our calcium assay results highlight the involvement of the calcium ion in the light emission process of both *P. phosphorea* and *F. quadrangularis*. Results obtained for the calcium ionophore A23187 reveal that the ion action does not result from intracellular calcium storage but rather is provided by external calcium input. Moreover, calcium is shown to be essential for the physiological luminescent response through adrenaline application. Pieces of evidence of calcium involvement in anthozoan luminescence were already described for *R. reniformis* and *V. cynomorium* [27,28].

These results let us assume a conservation of the coelenterazine-dependent *Renilla*-like luciferase bioluminescent system, involving also a CBP, across luminous Pennatulaceans (**Table S1**; [8]). The involvement of GFP appears species-dependent, with only a few species emitting blue light (**Table S1**; [8]). Nevertheless, deeper investigations are needed to fully apprehend the conservation of those actors across the diversity of luminous pennatulaceans.

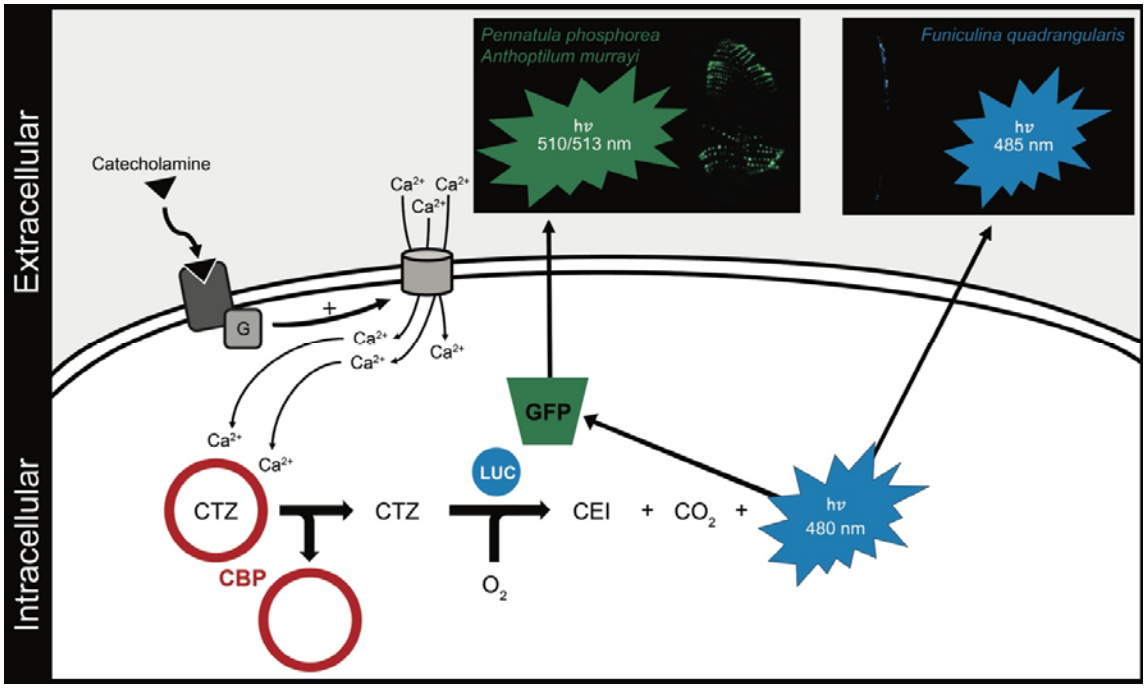

Figure 9: Schematic representation of the putative pathway driving the luminescence production in sea pens. Elements of this pathway have been compiled from the present results and the literature [13,14,17,21-25,32-36]. CBP, coelenterazine-binding protein; CEI, coelenteramide; CTZ, coelenterazine; G, G-protein; GFP, green fluorescent protein; LUC, luciferase. The clear colocalization of specific molecular actors (*e.g.,* catecholaminergic receptors, CBP, GFP, LUC) still needs to be established to confirm the following predicted pathway.

A hypothetical scheme of the generalized pathway could be established using our results and the literature on the pennatulacean luminescence mechanism (**Figure 9**). The first step is the activation of catecholaminergic receptors through the binding of biogenic amines (mainly adrenaline and noradrenaline [35,36]), which will release an intracellular-associated G-protein [85,86]. G-protein could be involved in a large variety of intracellular pathways [87], some of which involve increasing intracellular calcium (via direct or indirect activation of calcium channels) [88-91]. This intracellular calcium increase will lead to the release of the coelenterazine through the binding of this ion on the CBP, leaving this luciferin free to react with luciferase in the presence of oxygen to produce blue light around 480 nm [9-11,16,21-25,27]. For pennatulaceans lacking GFP (*e.g., F. quadrangularis*), this scheme ends here with the direct emission in blue color, while for those displaying GFP expression, the blue light is captured by this specific fluorescent protein and reemitted in green wavelength [22], such as for *P. phosphorea*. Future research is needed to validate this hypothetical scheme, and further investigations will be conducted to establish the functional activities of all these components in less-studied sea pens. Astonishingly, even if attempts were made on other anthozoans over the past decades, the *Renilla* bioluminescence system remains the only isolated and cloned system [14,16,22-25,27]. Despite the demonstrated widespread uses of the sea pansy bioluminescent system in biotechnology and biomedicine [*e.g.,* 92-94], the *Renilla* luciferase stands as the only one of the most commercially

employed gene reporters in biomolecular sciences. Nonetheless, in the *Renilla* bioluminescence system, the exact action mode of CBP and calcium is not fully apprehended [29,95]. Considering these facts, our introspection into the bioluminescent system of other luminous pennatulaceans could be of great use for new biotechnological advances. Our results provided a better understanding of the evolution of the bioluminescence system and associated molecules from these enigmatic benthic sessile organisms.

Supplemental data captions

Table S1. General overview of the bioluminescent knowledge among luminous anthozoans. All data were extracted from the literature (only scientific data described for species down to the species level have been taken into account to minimize generalizations). CBP, coelenterazine-binding protein; GFP, green fluorescent protein.

Table S2. Primers designed for *P. phosphorea* luciferase validation.

Table S3. Experiment protocol for the calcium assays.

Table S4. Description of the output sequenced data. Q20 percentage is the proportion of nucleotides with a quality value larger than 20 in reads. GC percentage is the proportion of guanidine and cytosine nucleotides among total nucleotides.

Table S5. Summary statistics of assemblies for *Pennatula phosphorea* pinnules, rachis, peduncle, and *Anthoptilum murrayi* transcriptomes.

Table S6. Transcript expression values (FPKM values) and public database sequences used during transcriptomic and phylogenetic analyses.

Figure S1: Luminometric measurements performed on the different area of *Pennatula phosphorea*. (A) schematic representation of *P. phosphorea* with the different areas (upper, middle, lower) of the pinnules and rachis. (B) Mean coelenterazine content recorded and (C) luciferase activity for the different pinnule areas. (D) Mean coelenterazine content recorded and (E) luciferase activity for the different rachis areas.

Figure S2: Biochemical assays following luminous parameters activity on *Pennatula phosphorea* pinnules (A, B, C) and rachis (D, E, F) during 1 year without coelenterazine supply. Mean total light emission after KCl applications (A, D), mean coelenterazine content (B, E), and mean maximal light emission during luciferase activity experiments (C, D). Different lettering indicates statistical differences. The timing corresponds to experiments performed on wild-caught specimens (T0) after 6 months (T6) and twelve months of captivity (T12).

Figure S3: Sequence alignments. (A) Alignment of the retrieved luciferases with a highlight on the conserved catalytic sites. (B) Alignment of the retrieved green fluorescent protein sequences. (C) Alignement of the retrieved coelenterazine-binding protein sequences.

Figure S4. Luciferase immunoblots on *Pennatula phosphorea* tissues (rachis, Ra; peduncle, Ped; and pinnule, Pin).

Figure S5. Total light emission (Ltot) after KCl applications with three different calcium concentrations in the medium. Experiments were performed on (A) pinnules, and (B) rachis of *Pennatula phosphorea*. ASW, artificial seawater; 0, 10, 20 correspond to the calcium concentration (mM) in the medium.

File S1: FASTA file of the retrieved Clade A luciferase sequences

File S2: FASTA file of the retrieved green fluorescent protein sequences

File S3: FASTA file of the retrieved coelenterazine-binding protein sequences

Acknowledgment

The authors acknowledge U. Schwarz, captain of the Alice vessel, and the skillful members of the Kristineberg Center (Goteborg University, Sweden) for their help during the *Pennatula* and *Funiculina* collection; and commandant J. Rezende and the crew of the R/V Alpha Crucis (Instituto Oceanográfico, USP). The authors also thank M. Jacquet for contributing to the study during his master's thesis and C. Pels, ELIV laboratory technician who maintained the organisms in the aquaria at the Marine Biology Laboratory - UCLouvain. The authors also want to thank T. Wiegand from the mobile lab (TREC- EMBL) for her help in visualizing coelenterazine autofluorescence and immunolabeling in the wild-caught specimens. The authors also thank J. Mallefet for his helpful advice and help during the first organisms sampling and all along the experiments.

LD is a postdoctoral researcher at the Université de Louvain - UCLouvain, GG is a Ph.D. student at Universidade de São Paulo - USP, CC is a Ph.D. student under an FRIA fellowship, LB is a postdoctoral researcher at the Université de Louvain - UCLouvain, RR is an academic professor at UCLouvain, MRSM is an academic professor at Universidade de São Paulo - USP, MM is group leader at the Masaryk University, DTA is an adjunct professor at Federal University of ABC, SD is a Senior Lecturer and Associate professor at the University of Gothenburg, AGO is an assistant professor at Yeshiva University, and JD is a postdoctoral researcher at FNRS. This study is the contribution of BRC#422 of the Biodiversity Research Center (UCLouvain) from the Earth and Life Institute Biodiversity (ELIV) and the “Centre Interuniversitaire de Biologie Marine” (CIBIM).

Competing interests

No competing interests declared

Data availability

Transcriptome raw reads were uploaded as Sequence Reads Archives (SRA): *A. murrayi* (PRJNA1144931), *P. phosphorea* (PRJNA1152785). The unigene annotation tables are accessible from the corresponding author upon request.

Funding

This work was supported by an F.R.S.-FNRS grant (T.0169.20) awarded to the Université de Louvain – UCLouvain Marine Biology Laboratory and the Université de Mons Biology of Marine Organisms and Biomimetics Laboratory, by the Czech Science Foundation (GA22-09853S), and by the Czech Ministry of Education, Youth and Sports (RECETOX RI LM2023069, e-INFRA LM2018140). The research leading to these results also received funding from the European Union's Horizon 2020 research and innovation program under grant agreement No 730984, ASSEMBLE Plus project. This study was financed in part by the Coordenação de Aperfeiçoamento de Pessoal de Nível Superior - Brasil (CAPES) - Finance Code 88887.605088/2021-00; Fundação de Amparo à Pesquisa do Estado de São Paulo (FAPESP 2017/12909-4, 2020/07600-7), and Yeshiva University Start-up Fund..

Author contributions

LD, CC, and SD collected the *P. phosphorea* and *F. quadrangularis* samples, and GG and MRSM sampled *A. murrayi*. Data collection and analyses were performed by LD, CC, LB, GG, AO and JD. Transcriptome analyses were performed by LD, GG, DTA, AO, and JD. Phylogenetic analyses were performed by JD. Structural analyses were performed by MM. The project was supervised by RR, SD, AO, and JD. The original manuscript was written by LD, GG, CC, AO, and JD. All the authors reviewed and approved the final version.

Reference

1. Shimomura O, Yampolsky IV. 2019 *Bioluminescence: chemical principles and methods*. 3rd edition (Singapore: World Scientific Publishing), 1–556.
2. Haddock SHD, Moline MA, Case JF. 2010 Bioluminescence in the sea. *Ann. Rev. Mar. Sci.* **2**, 443-493. (https://doi.org/10.1146/annurev-marine-120308-081028)
3. Delroisse J, Duchatelet L, Flammang P, Mallefet J. 2021 Leaving the dark side? Insights into the evolution of luciferases. *Front. Mar. Sci.* **8**, 673620. (https://doi.org/10.3389/fmars.2021.673620)
4. Fleiss A, Sarkisyan KS. 2019 A brief review of bioluminescent systems. *Curr. Genet.* **65**, 877-882. (https://doi.org/10.1007/s00294-019-00951-5)
5. Hastings JW. 1996 Chemistries and colors of bioluminescent reactions: a review. *Gene* **173(1)**, 5-11. (https://doi.org/10.1016/0378-1119(95)00676-1)
6. Wilson T, Hastings JW. 2012 *Bioluminescence: living lights, lights for living*. Harvard University Press.
7. Kaskova ZM, Tsarkova AS, Yampolsky IV. 2016 1001 lights: luciferins, luciferases, their mechanisms of action and applications in chemical analysis, biology and medicine. *Chem. Soc. Rev.* **45**, 6048-6077. (https://doi.org/10.1039/C6CS00296J)

8. Duchatelet L, Dupont S. 2024 Marine eukaryote bioluminescence: a review of species and their functional biology. *Mar. Life Sci. & Technol.* **2024**, 1-16. (https://doi.org/10.1007/s42995-024-00250-0)
9. Cormier MJ. 1960 Studies of the bioluminescence of *Renilla reniformis*: I. Requirements for luminescence in extracts and characteristics of the system. *Biochimica et Biophysica Acta* **42**, 333-343. (https://doi.org/10.1016/0006-3002(60)90797-6)
10. Matthews JC, Hori K, Cormier MJ. 1977 Purification and properties of *Renilla reniformis* luciferase. *Biochemistry* **16(1)**, 85-91. (https://doi.org/10.1021/bi00620a014)
11. Lorenz WW, McCann RO, Longiaru M, Cormier MJ. 1991 Isolation and expression of a cDNA encoding *Renilla reniformis* luciferase. *PNAS* **88(10)**, 4438-4442. (https://doi.org/10.1073/pnas.88.10.4438)
12. Loening AM, Fenn TD, Gambhir SS. 2007 Crystal structures of the luciferase and green fluorescent protein from *Renilla reniformis*. *J. Mol. Biol.* **374(4)**, 1017-1028. (https://doi.org/10.1016/j.jmb.2007.09.078)
13. Bessho-Uehara M, Francis WR, Haddock SHD. 2020 Biochemical characterization of diverse deep-sea anthozoan bioluminescence systems. *Mar. Biol.* **167**, 114. (https://doi.org/10.1007/s00227-020-03706-w)
14. Schenkmayerova A, Toul M, Pluskal D, Baatallah R, Gagnot G, Pinto GP, Santana VT, et al. 2023 Catalytic mechanism for *Renilla*-type luciferases. *Nat. Catal.* **6**, 23-38. (https://doi.org/10.1038/s41929-022-00895-z)
15. DeLeo D, Bessho-Uehara M, Haddock SHD, McFadden CS, Quattrini AM. 2024 Evolution of bioluminescence in Anthozoa with emphasis on Octocorallia. *Proc. R. Soc. B.* **291**, 20232626. (https://doi.org/10.1098/rspb.2023.2626)
16. Inoue S, Kakoi H, Murata M, Goto T, Shimomura O. 1977 Complete structure of *Renilla* luciferin and luciferyl sulfate. *Tetrahedron Lett.* **18(31)**, 2685-2688. (https://doi.org/10.1016/S0040-4039(01)83046-X)
17. Cormier MJ, Hori K, Karkhanis YD, Anderson JM, Wampler JE, Morin JG, Hastings JW. 1973 Evidence for similar biochemical requirements for bioluminescence among coelenterates. *J. Cell. Physiol.* **81(2)**, 291-297. (https://doi.org/10.1002/jcp.1040810218)
18. Delroisse J, Ullrich-Lüter E, Blaue S, Ortega-Martinez O, Eeckhaut I, Flammang P, Mallefet J. 2017 A puzzling homology: a brittle star using a putative cnidarian-type luciferase for bioluminescence. *Open Biol.* **7(4)**, 160300. (https://doi.org/10.1098/rsob.160300)
19. Tessler M, Gaffney JP, Oliveira AG, Guarnaccia A, Dobi KC, Gujarati NA, et al. 2020 A putative chordate luciferase from a cosmopolitan tunicate indicates convergent bioluminescence evolution across phyla. *Sci. Rep.* **10**, 17724. (https://doi.org/10.1038/s41598-020-54373446-w)
20. Lau ES, Majerova M, Hensley NM, Mukherjee A, Vasina M, Pluskal D, Damborsky J, Prokop Z, Delroisse J, Bayaert W-S, Parey E, Oliveri P, Marletaz F, Marek M, Oakley TH. 2024. Functional characterization of luciferase in a brittle star indicates parallel

1135 evolution influenced by genomic availability of haloalkane dehalogenase. *bioRxiv*
1136 2024.10.14.618359. (https://doi.org/10.1101/2024.10.14.618359)
1137 21. Anderson J, Charbonneau H, Cormier MJ. 1974 Mechanism of calcium induction of
1138 *Renilla* bioluminescence. Involvement of a calcium-triggered luciferin binding protein.
1139 *Biochemistry* **13(6)**, 1195-1200. (https://doi.org/10.1021/bi00703a602)
1140 22. Ward WW, Cormier MJ. 1979 Energy transfer protein in coelenterate bioluminescence.
1141 Characterization of the *Renilla* green-fluorescent protein. *J. Biol. Chem.* **254(3)**, 781-
1142 788.
1143 23. Kumar S, Harrylock M, Walsh KA, Cormier MJ, Charbonneau H. 1990 Amino acid
1144 sequence of the Ca^{2+}-triggered luciferin binding protein of *Renilla reniformis*. *FEBS Lett.*
1145 **268(1)**, 287-290. (https://doi.org/10.1016/0014-5793(90)81029-N)
1146 24. Inouye S. 2007 Expression, purification and characterization of calcium-triggered
1147 luciferin-binding protein of *Renilla reniformis*. *Protein Expr. Purif.* **52(1)**, 66-73.
1148 (https://doi.org/10.1016/j.pep.2006.07.028)
1149 25. Titushin MS, Markova SV, Frank LA, Malikova NP, Stepanyuk GA, Lee J, Vysotski ES.
1150 2008 Coelenterazine-binding protein of *Renilla muelleri* : cDNA cloning,
1151 overexpression, and characterization as a substrate of luciferase. *Photochem.*
1152 *Photobiol. Sci.* **7**, 189-196. (https://doi.org/10.1039/b713109g)
1153 26. Ogoh K, Kinebuchi T, Murai M, Takahashi T, Ohmiya Y, Suzuki H. 2013 Dual-color-
1154 emitting green fluorescent protein from the sea cactus *Cavernularia obesa* and its use
1155 as a pH indicator for fluorescent microscopy. *Luminescence* **28(4)**, 582-591.
1156 (https://doi.org/10.1002/bio.2497)
1157 27. Henry J-P, Ninio M. 1978 Control of the Ca^{2+}-triggered bioluminescence of *Veretillum*
1158 *cynomorium* lumisomes. *Biochimica et Biophysica acta* **504(1)**, 40-59.
1159 (https://doi.org/10.1016/0005-2728(78)90005-1)
1160 28. Charbonneau H, Cormier MJ. 1979 Ca^{2+}-induced bioluminescence in *Renilla reniformis*.
1161 Purification and characterization of a calcium-triggered luciferin-binding protein. *J.*
1162 *Biol. Chem.* **254(3)**, 769-780. (https://doi.org/10.1016/S0021-9258(17)37872-9)
1163 29. Stepanyuk GA, Liu Z-J, Vysotski ES, Lee J, Rose JP, Wang B-C. 2008 Structure based
1164 mechanism of the Ca^{2+}-induced release of coelenterazine from the *Renilla* binding
1165 protein. *Proteins* **74(3)**, 583-593. (https://doi.org/10.1002/prot.22173)
1166 30. Nicol JAC. 1955 Observations on luminescence in *Renilla* (Pennatulacea). *J. Exp. Biol.*
1167 **51232(2)**, 299-320.
1168 31. Davenport D, Nicol JAC. 1956 Observations on luminescence in sea pens
1169 (Pennatulacea). *Proc. R. Soc. B* **144(917)**, 480-496.
1170 (https://doi.org/10.1098/rspb.1956.0005)
1171 32. Wampler JE, Karkhanis YD, Morin JG, Cormier MJ. 1973 Similarities in the
1172 bioluminescence from the Pennatulacea. *Biochimica et Biophysica Acta* **314**, 104-109.
1173 (https://doi.org/10.1016/0005-2728(73)90068-6)

1174 33. Satterlie RA, Anderson PAV, Case JF. 1980 Colonial coordination on anthozoans:
1175 Pennatulacea. *Mar. Behav. Physiol.* **7**, 25-46.
1176 (https://doi.org/10.1080/10236248009386969)
1177 34. Germain G, Anctil M. 1988 Luminescent activity and ultrastructural characterization of
1178 photocytes dissociated from the coelenterate *Renilla köllikeri*. *Tissue and Cell* **20(5)**,
1179 701-720. (https://doi.org/10.1016/0040-8166(88)90017-1)
1180 35. Anctil M, Boulay D, Larivière L. 1982 Monoaminergic mechanisms associated with
1181 control of luminescence and contractile activities in the coelenterate, *Renilla köllikeri*.
1182 *J. Exp. Zool.* **223(1)**, 11-24. (https://doi.org/10.1002/jez.1402230103)
1183 36. Duchatelet L, Coubris C, Pels C, Dupont S, Mallefet J. 2023 Catecholamine involvement
1184 in the bioluminescence control of two species of Anthozoans. *Life* **13(9)**, 1798.
1185 (https://doi.org/10.3390/life13091798)
1186 37. Morin JG. 1976 Probable functions of bioluminescence in the Pennatulacea (Cnidaria,
1187 Anthozoa). In: Mackie GO. (Ed) *Coelenterate Ecology and Behavior*. Springer, Boston,
1188 MA, USA. (https://doi.org/10.1007/978-1-4757-9724-4_65)
1189 38. Delroisse J, Mallefet J, Flammang P. 2016 *De novo* adult transcriptomes of two
1190 European brittle stars: spotlight on opsin-based photoreception. *PLoS ONE* **11(4)**,
1191 e0152988. (https://doi.org/10.1371/journal.pone.0152988)
1192 39. Delroisse J, Duchatelet L, Flammang P, Mallefet J. 2018 *De novo* transcriptome
1193 analyses provide insights into opsin-based photoreception in the lanternshark
1194 *Etmopterus spinax*. *PLoS ONE* **13(12)**, e0209767.
1195 (https://doi.org/10.1371/journal.pone.0209767)
1196 40. Delroisse J, Duchatelet L, Flammang P, Mallefet J. 2021 Photophore distribution and
1197 enzymatic diversity within the photogenic integument of the cookie-cutter shark
1198 *Isistius brasiliensis* (Chondrichthyes: Dalatiidae). *Front. Mar. Sci.* **8**, 627045.
1199 (https://doi.org/10.3389/fmars.2021.627045)
1200 41. Cock PJA, Fields CJ, Goto N, Heuer ML, Rice PM. 2010 The Sanger FASTQ file format for
1201 sequences with quality scores and the Solexa/Illumina FASTQ variants. *Nucleic Acids*
1202 *Res.* **38(6)**, 1767-1771. (https://doi.org/10.1093/nar/gkp1137)
1203 42. Grabherr MG, Haas BJ, Yassour M, Levin JZ, Thompson DA, Amit I, et al. 2011 Full-
1204 length transcriptome assembly from RNA-Seq data without a reference genome. *Nat.*
1205 *Biotechnol.* **29**, 644-652. (https://doi.org/10.1038/nbt.1883)
1206 43. Pertea G, Huang X, Liang F, Antonescu V, Sultana R, Karamycheva S, et al. 2002 TIGR
1207 gene indices clustering tools (TGICL): a software system for fast clustering of large EST
1208 datasets. *Bioinformatics* **19(5)**, 651-652.
1209 (https://doi.org/10.1093/bioinformatics/btg034)
1210 44. Das S, Shyamal S, Durica DS. 2016 Analysis of annotation and differential expression
1211 methods used in RNA-seq studies in crustacean systems. *Integr. Comp. Biol.* **56(6)**,
1212 1067-1079. (https://doi.org/10.1093/icb/icw117)
1213 45. Altschul SF, Gish W, Miller W, Myers EW, Lipman DJ. 1990 Basic local alignment search
1214 tool. *J. Mol. Biol.* **215(3)**, 403-410. (https://doi.org/10.1016/S0022-2836(05)80360-2)

1215 46. Buchfink B, Xie C, Huson DH. 2014 Fast and sensitive protein alignment using
1216 DIAMOND. *Nat. Methods* **12**, 59-60. (https://doi.org/10.1038/nmeth.3176)
1217 47. Conesa A, Götz S, García-Gómez JM, Terol J, Talón M, Robles M. 2005 Blast2GO: a
1218 universal tool for annotation, visualization and analysis in functional genomics
1219 research. *Bioinformatics* **21(18)**, 3674-3676.
1220 (https://doi.org/10.1093/bioinformatics/bti610**)**
1221 48. Quevillon E, Silventoinen V, Pillai S, Harte N, Mulder N, Apweiler R, Lopez R. 2005
1222 InterProScan: protein domains identifier. *Nucleic Acids Res.* **33**, W116-W120.
1223 (https://doi.org/10.1093/nar/gki442)
1224 49. Haas BJ, Papanicolaou A, Yassour M, Grabherr M, Blood PD, Bowden J, Couger MB,
1225 Eccles D, Li B, Lieber M, MacManes MD, Ott M, Orvis J, Pochet N, Strozzi F, Weeks N,
1226 Westerman R, William T, Dewey CN, Henschel R, LeDuc RD, Friedman N, Regev A. 2013
1227 *De novo* transcript sequence reconstruction from RNA-seq using the Trinity platform
1228 for reference generation and analysis. *Nat. Protoc.* **8**, 1494-1512.
1229 (https://doi.org/10.1038/nprot.2013.084)
1230 50. Kearse M, Moir R, Wilson A, Stones-Havas S, Cheung M, Sturrock S, et al. 2012
1231 Geneious Basic: an integrated and extendable desktop software platform for the
1232 organization and analysis of sequence data. *Bioinformatics* **28(12)**, 1647-1649.
1233 (https://doi.org/10.1093/bioinformatics/bts199)
1234 51. Woo J, Howell MH, von Arnim AG. 2009 Structure-function studies on the active site of
1235 the coelenterazine-dependent luciferase from *Renilla*. *Protein Sci.* **17(4)**, 725-735.
1236 (https://doi.org/10.1110/ps.073355508)
1237 52. McFadden CS, van Ofwegen LP, Quattrini AM. 2022 Revisionary systematics of
1238 Octocorallia (Cnidaria: Anthozoa) guided by phylogenomics. *Bulletin of the Society of*
1239 *Systematics Biologists* **1(3)**. (https://doi.org/10.18061/bssb.v1i3.8735)
1240 53. Labas YA, Gurskaya NG, Yanushevich YG, Fradkov AF, Lukyanov KA, Lukyanov SA, Matz
1241 MV. 2002 Diversity and evolution of the green fluorescent protein family. *Proc. Natl*
1242 *Acad. Sci.* **99(7)**, 4257-4261. (https://doi.org/10.1073/pnas.062552299)
1243 54. Alieva NO, Konzen KA, Field SF, Meleshkevitch EA, Hunt ME, Beltran-Ramirez V, Miller
1244 DJ, Wiedenmann J, Salih A, Matz MV. 2008 Diversity and evolution of coral fluorescent
1245 proteins. *PLoS ONE* **3(7)**, e2680. (https://doi.org/10.1371/journal.pone.0002680)
1246 55. Li G, Zhang QJ, Zhong J, Wang YQ. 2009 Evolutionary and functional diversity of green
1247 fluorescent proteins in cephalochordates. *Gene* **446(1)**, 41-49.
1248 (https://doi.org/10.1016/j.gene.2009.07.003)
1249 56. Shagin DA, Barsova EV, Yanushevich YG, Fradkov AF, Lukyanov KA, Labas YA, Semenova
1250 TN, Ugalde JA, Meyers A, Nunez JM, Widder EA, Lukyanov SA, Matz MV. 2004 GFP-like
1251 proteins as ubiquitous metazoan superfamily: evolution of functional features and
1252 structural complexity. *Mol. Biol. Evol.* **21(5)**, 841-850.
1253 (https://doi.org/10.1093/molbev/msh079)
1254 57. Schnitzler CE, Pang K, Powers ML, Reitzel AM, Ryan JF, Simmons D, Tada T, Park M,
1255 Gupta J, Brooks SY, Blakesley RW, Yokoyama S, Haddock SHD, Martindale MQ,

1256 Baxevanis AD. 2012 Genomic organization, evolution, and expression of photoprotein
1257 and opsin genes in *Mnemiopsis leidyi*: a new view of ctenophore photocytes. *BMC Biol.*
1258 **10**, 1-26. (https://doi.org/10.1186/1741-7007-10-107)
1259 58. Capella-Gutierrez S, Silla-Martinez JM, Gabaldon T. 2009 trimAl: a tool for automated
1260 alignment trimming in large-scale phylogenetic analyses. *Bioinformatics* **25**, 1972-
1261 1973. (https://doi.org/10.1093/bioinformatics/btp348)
1262 59. Nguyen LT, Schmidt HA, Von Haeseler A, Minh BQ. 2015 IQ-TREE: a fast and effective
1263 stochastic algorithm for estimating maximum-likelihood phylogenies. *Mol. Biol. Evol.*
1264 **32(1)**, 268-274. (https://doi.org/10.1093/molbev/msu300)
1265 60. Posada D, Crandall KA. 1998 MODELTEST: testing the model of DNA substitution.
1266 *Bioinformatics (Oxford, England)* **14(9)**, 817-818.
1267 (https://doi.org/10.1093/bioinformatics/14.9.817)
1268 61. Nicol JAC. 1958 Observations on the luminescence of *Pennatula phosphorea*, with a
1269 note on the luminescence of *Virgularia mirabilis*. *J. Mar. Biol. Assoc. UK* **37**, 551–563.
1270 (https://doi.org/10.1017/S0025315400005610)
1271 62. Rahnama S, Saffar B, Kahrani Z.F, Nazari M, Emamzadeh R. 2017 Super RLuc8: a novel
1272 engineered *Renilla* luciferase with a red-shifted spectrum and stable light emission.
1273 *Enzym. Microb. Technol.* **96**, 60-66. (https://doi.org/10.1016/j.enzmictec.2016.09.009)
1274 63. Khoshnevisan G, Emamzadeh R, Nazari M, Rasa SMM, Sariri R, Hassani L. 2018 Kinetics,
1275 structure, and dynamics of *Renilla* luciferase solvated in binary mixtures of glycerol and
1276 water and the mechanism by which glycerol obstructs the enzyme emitter site. *Int. J.*
1277 *Biol. Macromol.* **117**, 617-624. (https://doi.org/10.1016/j.ijbiomac.2018.05.160)
1278 64. Mallefet J, Duchatelet L, Coubris C. 2020 Bioluminescence induction in the ophiuroid
1279 *Amphiura filiformis* (Echinodermata). *J. Exp. Biol.* **223(4)**, jeb218719.
1280 (https://doi.org/10.1242/jeb.218719)
1281 65. Mallefet J, Martinez-Soares P, Eléaume M, O'Hara T, Duchatelet L. 2023 New insights
1282 on crinoid (Echinodermata; Crinoidea) bioluminescence. *Front. Mar. Sci.* **10**, 1136138.
1283 (https://doi.org/10.3389/fmars.2023.1136138)
1284 66. Loening AM, Fenn TD, Wu AM, Gambhir SS. 2006 Consensus guided mutagenesis of
1285 *Renilla* luciferase yields enhanced stability and light output. *Protein Eng. Des. Sel.*
1286 **19(9)**, 391–400. (https://doi.org/10.1093/protein/gzl023)
1287 67. Nandi A, Zhang A, Chu ZT, Xie WJ, Xu Z, Dong S, Warshel A. 2024 Exploring the light-
1288 emitting agents in *Renilla* luciferases by an effective QM/MM approach. *J. Am. Chem.*
1289 *Soc*. **46(20)**, 13875–13885. (https://doi.org/10.1021/jacs.4c00963)
1290 68. Tsuji FI, Ohmiya Y, Fagan TF, Toh H, Inouye S. 1995 Molecular evolution of the Ca^{2+}-
1291 binding photoproteins of the hydrozoa. *Photochem. Photobiol.* **62(4)**, 657-661.
1292 (https://doi.org/10.1111/j.1751-1097.1995.tb08713.x)
1293 69. Powers ML, McDermott AG, Shaner NC, Haddock SHD. 2013 Expression and
1294 characterization of the calcium-activated photoprotein from the ctenophore
1295 *Bathocyroe fosteri*: Insights into light-sensitive photoproteins. *Biochem. Biophys. Res.*
1296 *Commun.* **431(2)**, 360-366. (https://doi.org/10.1016/j.bbrc.2012.12.026)

70. Burakova LP, Stepanyuk GA, Eremeeva EV, Vysotski ES. 2016 Role of certain amino acid residues of the coelenterazine-binding cavity in bioluminescence of light-sensitive Ca^{2+}-regulated photoprotein berovin. *Photochem. Photobiol. Sci.* **15**, 691-704. (https://doi.org/10.1039/c6pp00050a)
71. Burakova LP, Vysotski ES. 2019 Recombinant Ca2+-regulated photoproteins of ctenophores: Current knowledge and application prospects. *Appl. Microbiol. Biotechnol.* **103**, 5929-5946. (https://doi.org/10.1007/s00253-019-09939-0)
72. Jumper J, Evans R, Pritzel A, Green T, Figurnov M, Ronneberger O, *et al*. 2021 Highly accurate protein structure prediction with AlphaFold. *Nature* **596**, 583-589. (https://doi.org/10.1038/s41586-021-03819-2)
73. Abramson J, Adler J, Dunger J, Evans R, Green T, Pritzel A, *et al.* 2024 Accurate structure prediction of biomolecular interactions with AlphaFold 3. *Nature* **630**, 493-500. (https://doi.org/10.1038/s41586-024-07487-w)
74. Stepanyuk GA, Liu Z-J, Markova SS, Frank LA, Lee J, Vysotski ES, Wang B-C. 2008 Crystal structure of coelenterazine-binding protein from *Renilla muelleri* at 1.7Å: Why it is not a calcium-regulated photoprotein. *Photochem. Photobiol. Sci.* **7**, 442-447. (https://doi.org/10.1039/b716535h)
75. Buskey EJ, Stearns DE. 1991 The effects of starvation on bioluminescence potential and egg release of the copepod *Metridia longa*. *J. Plankton Res.* **13(4)**, 885-893. (https://doi.org/10.1093/plankt/13.4.885)
76. Thomson CM, Herring PJ, Campbell AK. 1995 Evidence for *de novo* biosynthesis of coelenterazine in the bioluminescent midwater shrimp, *Systellaspis debilis* C. *J. Mar. Biol. Assoc. U.K.* **75(1)**, 165-171. (https://doi.org/10.1017/S0025315400015277)
77. Oba Y, Kato S-I, Ojika M, Inouye S. 2009 Biosynthesis of coelenterazine in the deep-sea copepod, *Metridia pacifica*. *Biochem. Biophys. Res. Commun.* **390(3)**, 684-688. (https://doi.org/10.1016/j.bbrc.2009.10.028)
78. Bessho-Uehara M, Huang W, Patry WL, Browne WE, Weng J-K, Haddock SHD. 2020 Evidence for *de novo* biosynthesis of the luminous substrate coelenterazine in ctenophores. *iScience* **23(12)**, 101859. (https://doi.org/10.1016/j.isci.2020.101859)
79. Francis WR, Shaner NC, Christianson LM, Powers ML, Haddock SHD. 2015 Occurrence of isopenicillin-N-synthase homologs in bioluminescent ctenophores and implications for coelenterazine biosynthesis. *PLoS ONE* **10(6)**, e0128742. (https://doi.org/10.1371/journal.pone.0128742)
80. Haddock SHD, Rivers TJ, Robison BH. 2001 Can coelenterates make coelenterazine? Dietary requirement for luciferin in cnidarian bioluminescence. *Proc. Ntl Acad. Sci.* **98(20)**, 11148-11151.(https://doi.org/10.1073/pnas.201329798)
81. Herring PJ. 1991 Observations on bioluminescence in some deep-water anthozoans. In *Coelenterate Biology: Recent Research on Cnidaria and Ctenophora, Proceedings of the Fifth International Conference on Coelenterate Biology*, Southampton, UK, 10–14 July 1989; Springer: Dordrecht, The Netherlands; pp. 573–579.

82. Coubris C, Duchatelet L, Delroisse J, Bayaert WS, Parise L, Eloy MC, Pels C, Mallefet J. 2024 Maintain the light, long-term seasonal monitoring of luminous capabilities in the brittle star *Amphiura filiformis*. *Sci. Rep.* **14**, 13238. (https://doi.org/10.1038/s41598-024-64010-x)
83. Herring P.J. 1978 Bioluminescence of invertebrates other than insects. In: Herring P.J. (ed), *Bioluminescence in action*, New York Academic Press, pp.199-240.
84. Inouye S, Watanabe K, Nakamura H, Shimomura O. 2000 Secretional luciferase of the luminous shrimp *Oplophorus gracilirostris*: cDNA cloning of a novel imidazopyrazinone luciferase. *FEBS Lett.* **481(1)**, 19-25. (https://doi.org/10.1016/S0014-5793(00)01963-3)
85. Kobilka B. 1992 Adrenergic receptors as models for G protein-coupled receptors. *Ann. Rev. Neurosci.* **15(1)**, 87-114. (https://doi.org/10.1146/annurev.ne.15.030192.000511)
86. Caron MG, Lefkowitz RJ. 1993 Catecholamine receptors: structure, function, and regulation. *Recent Prog. Horm. Res.* **1993**, 277-290. (https://doi.org/10.1016/B978-0-12-571148-7.50014-2)
87. Neves SR, Ram PT, Iyengar R. 2002 G protein pathways. *Science* **296(5573)**, 1636-1639. (https://doi.org/10.1126/science.1071550)
88. Brown AM, Birnbaumer L. 1988 Direct G protein gating of ion channels. *Am. J. Physiol. Heart Circ. Physiol.* **254(3)**, H401-H410. (https://doi.org/10.1152/ajpheart.1988.254.3.H401)
89. Hille B. 1994 Modulation of ion-channel function by G-protein-coupled receptors. *Trends Neurosci.* **17(12)**, 531-536. (https://doi.org/10.1016/0166-2236(94)90157-0)
90. Dolphin AC. 2003 G protein modulation of voltage-gated calcium channels. *Pharmacol. Rev.* **55(4)**, 607-627. (https://doi.org/10.1124/pr.55.4.3)
91. Tedford HW, Zamponi GW. 2006 Direct G protein modulation of Cav2 calcium channels. *Pharmacol. Rev.* **58(4)**, 837-862. (https://doi.org/10.1124/pr.58.4.11)
92. Roda A, Pasini P, Mirasoli M, Michelini E, Guardigli M. 2004 Biotechnological applications of bioluminescence and chemiluminescence. *Trends Biotechnol.* **22(6)**, 295-303. (https://doi.org/10.1016/j.tibtech.2004.03.011)
93. Kirkpatrick A, Xu T, Ripp S, Sayler G, Close D. 2019 Biotechnological advances in luciferase enzymes. *Bioluminescence-Analytical Applications and Basic Biology*, 1-23. (https://doi.org/10.5772/intechopen.85313)
94. Welsh DK, Kay SA. 2005 Bioluminescence imaging in living organisms. *Curr. Opin. Biotechnol.* **16(1)**, 73-78. (https://doi.org/10.1016/j.copbio.2004.12.006)
95. Kudryavtsev AN, Krasitskaya VV, Efremov MK, Zangeeva SV, Rogova AV, Tomilin FN, Frank LA. 2023 Ca^{2+}-trigerred coelenterazine-binding protein *Renilla*: Expected and unexpected features. *Int. J. Mol. Sci.* **24(3)**, 2144. (https://doi.org/10.3390/ijms24032144)

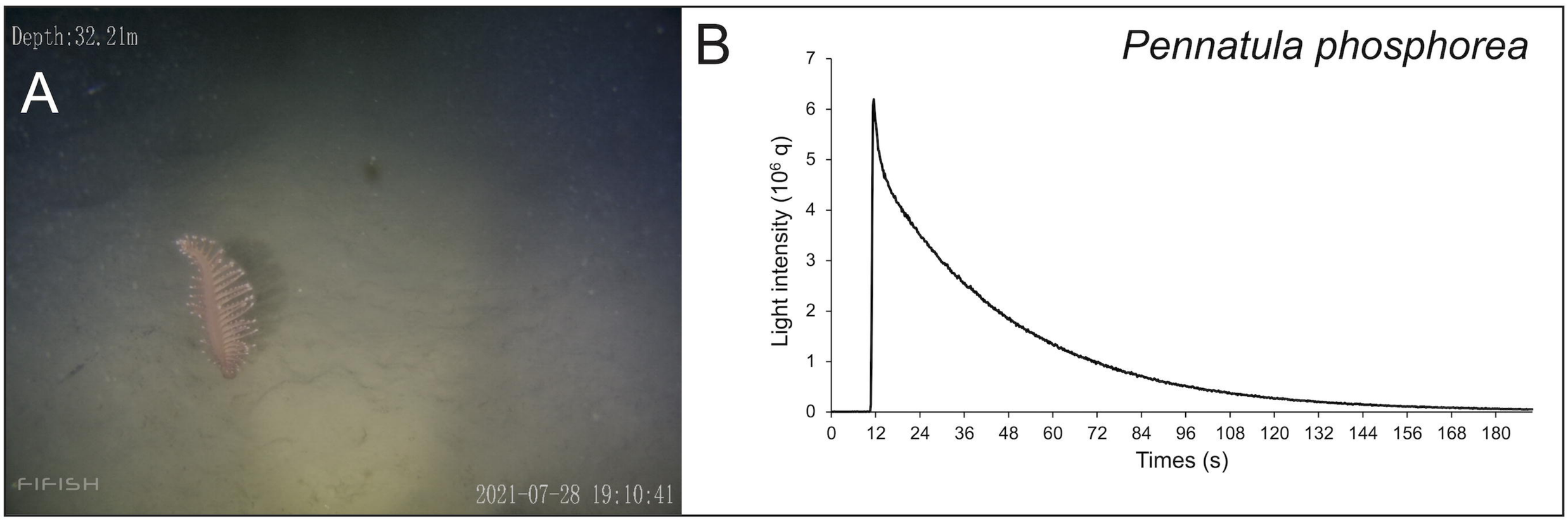
Depth:32.21m
A
FIFISH
2021-07-28 19:10:41
B
Pennatula phosphorea
Light intensity (10^6 q)
Times (s)

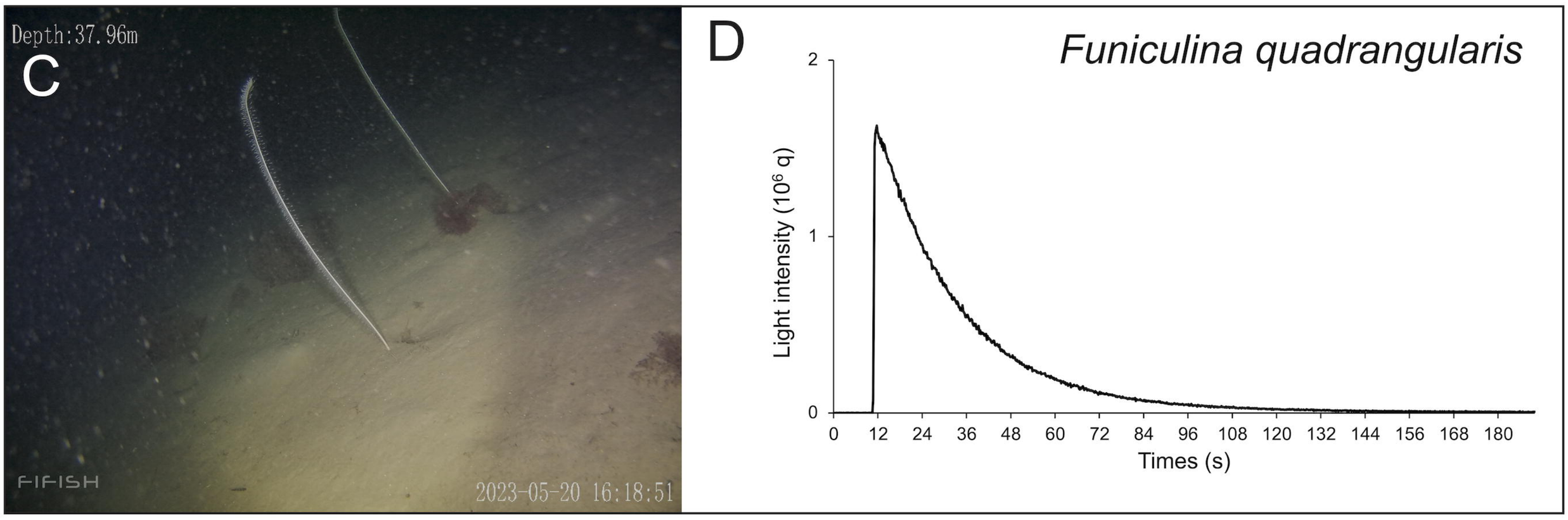
Depth:37.96m
C
FIFISH
2023-05-20 16:18:51
D
Funiculina quadrangularis
Light intensity (10^6 q)
Times (s)

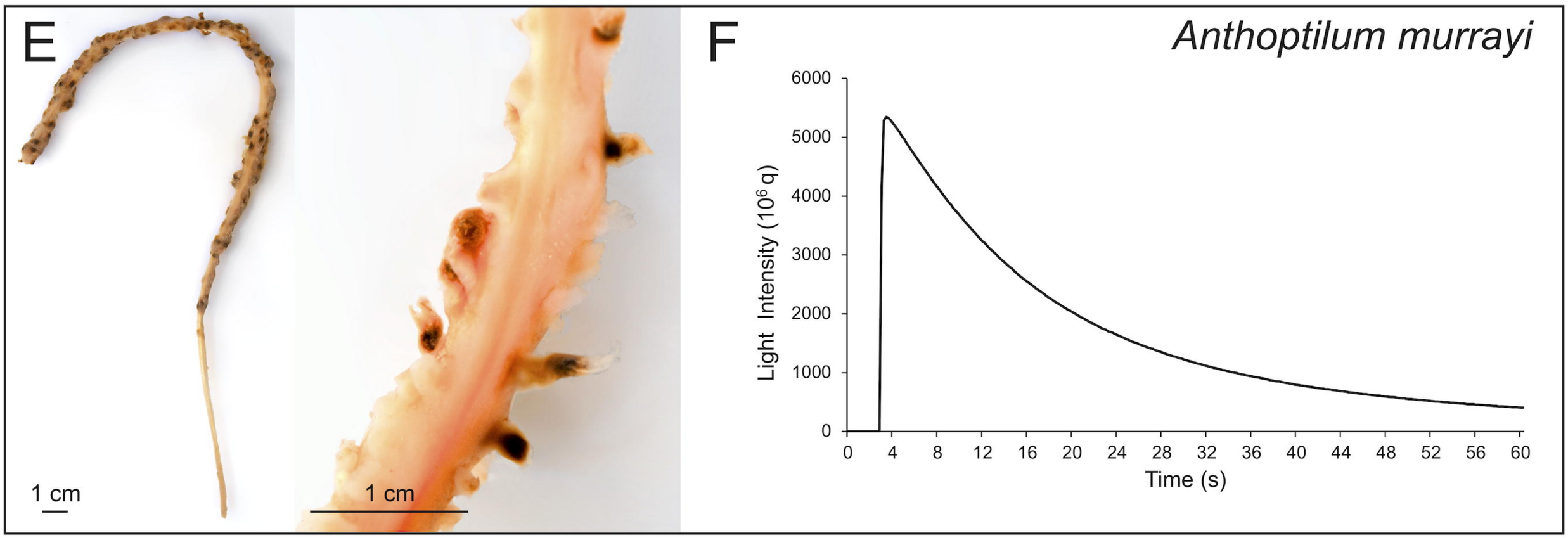
E
1 cm
1 cm
F
Anthoptilum murrayi
Light Intensity (10^6 q)
Time (s)

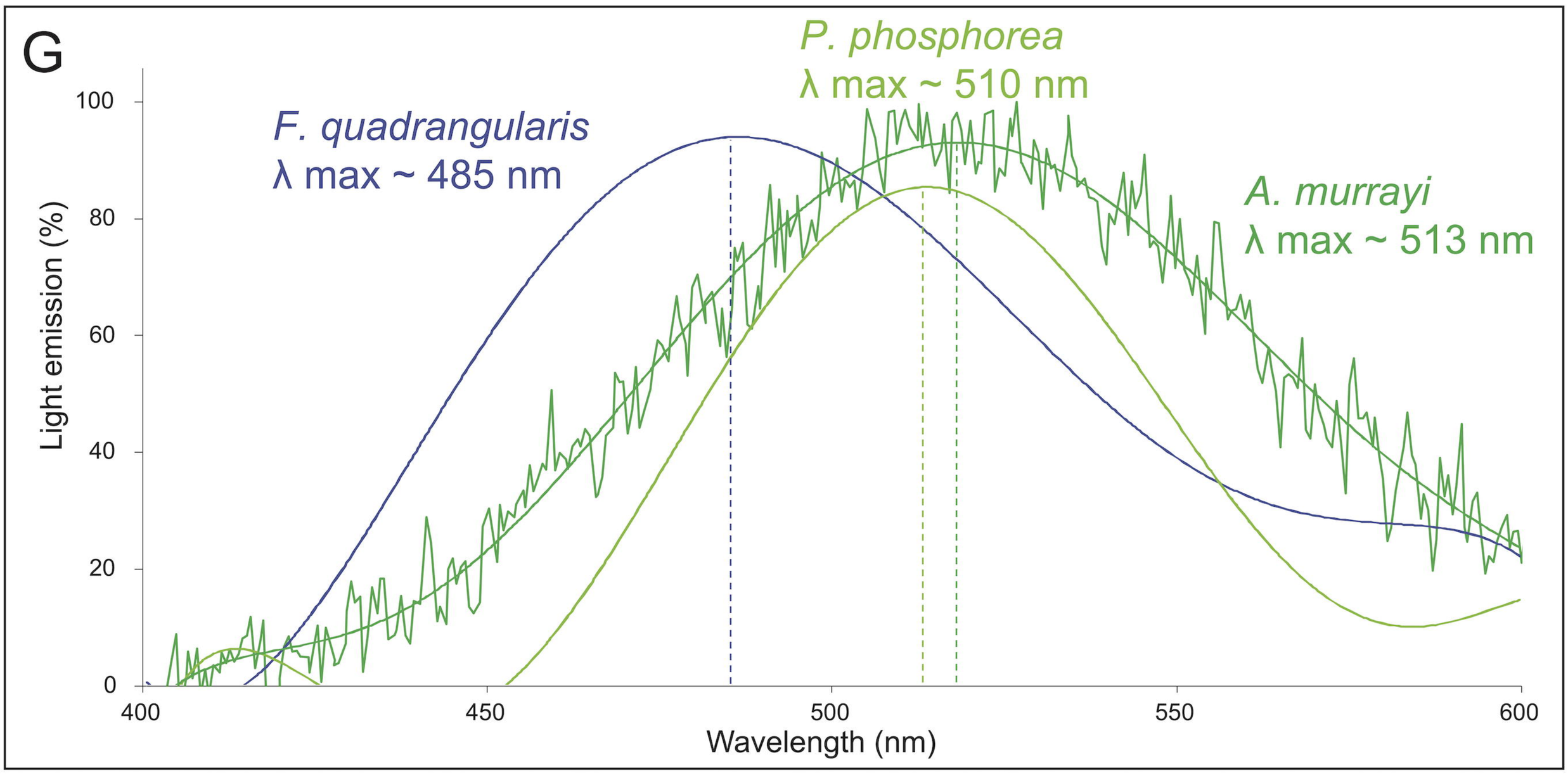
G
F. quadrangularis
λ max ~ 485 nm
P. phosphorea
λ max ~ 510 nm
A. murrayi
λ max ~ 513 nm
Light emission (%)
Wavelength (nm)

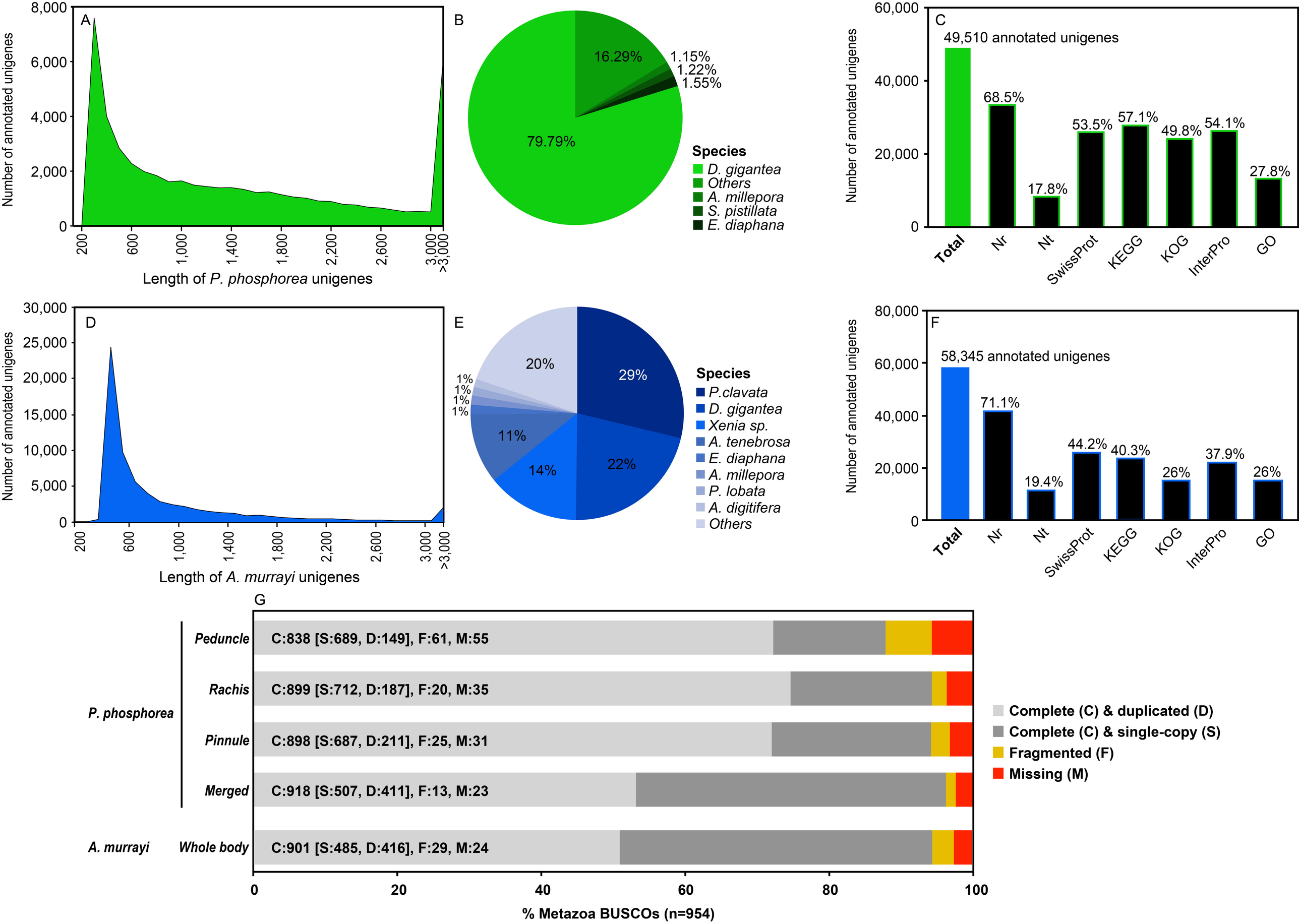
A
Number of annotated unigenes
8,000
6,000
4,000
2,000
0
200
600
1,000
1,400
1,800
2,200
2,600
3,000
>3,000
Length of P. phosphorea unigenes
B
16.29%
1.15%
1.22%
1.55%
79.79%
Species
D. gigantea
Others
A. millepora
S. pistillata
E. diaphana
C
49,510 annotated unigenes
68.5%
17.8%
53.5%
57.1%
49.8%
54.1%
27.8%
Total
Nr
Nt
SwissProt
KEGG
KOG
InterPro
GO
D
Length of A. murrayi unigenes
E
20%
29%
1%
1%
1%
1%
11%
14%
22%
Species
P.clavata
D. gigantea
Xenia sp.
A. tenebrosa
E. diaphana
A. millepora
P. lobata
A. digitifera
Others
F
58,345 annotated unigenes
71.1%
19.4%
44.2%
40.3%
26%
37.9%
26%
G
P. phosphorea
Peduncle
C:838 [S:689, D:149], F:61, M:55
Rachis
C:899 [S:712, D:187], F:20, M:35
Pinnule
C:898 [S:687, D:211], F:25, M:31
Merged
C:918 [S:507, D:411], F:13, M:23
A. murrayi
Whole body
C:901 [S:485, D:416], F:29, M:24
% Metazoa BUSCOs (n=954)
Complete (C) & duplicated (D)
Complete (C) & single-copy (S)
Fragmented (F)
Missing (M)

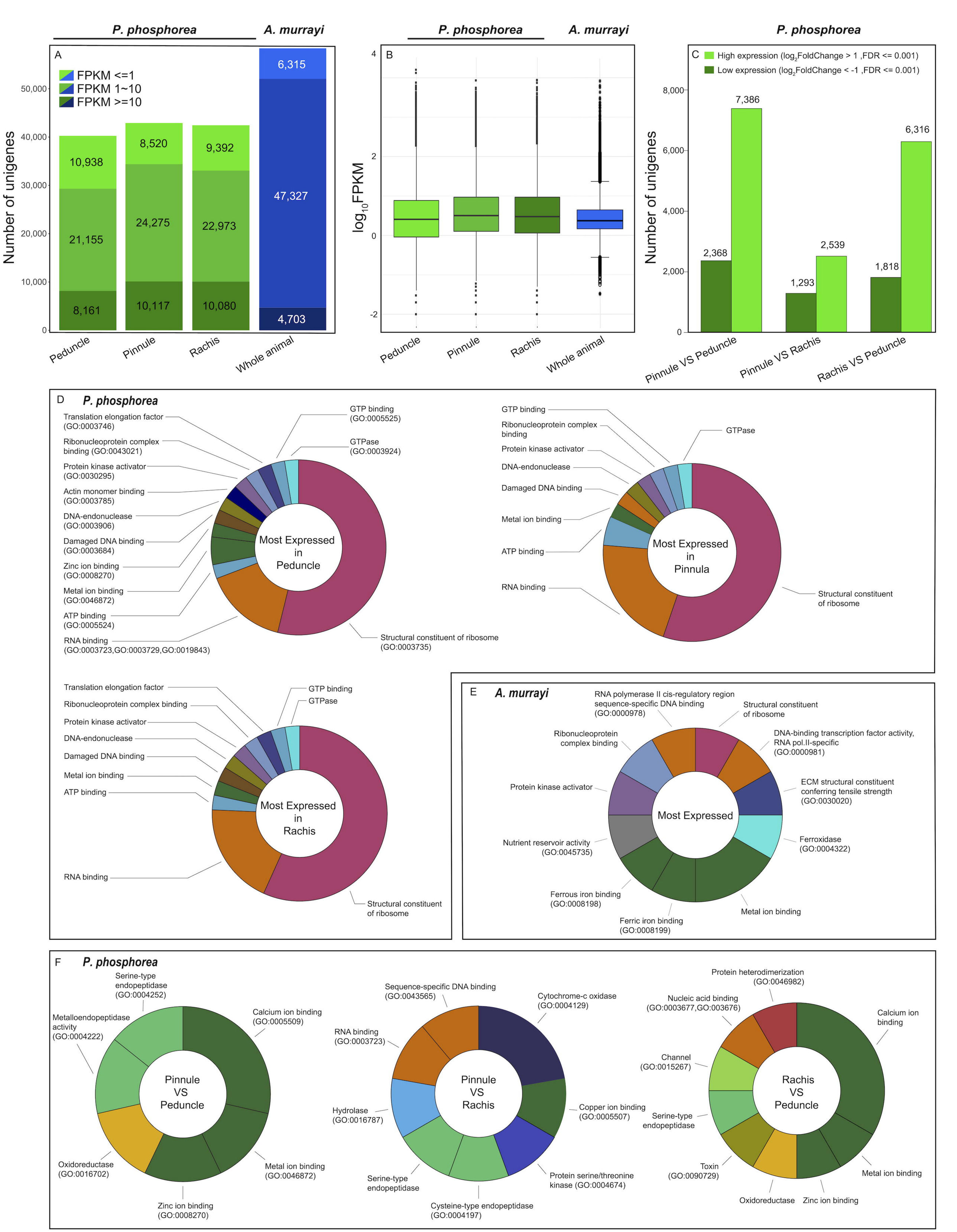
P. phosphorea
A. murrayi
A
FPKM <=1
FPKM 1~10
FPKM >=10
Number of unigenes
10,938
21,155
8,161
8,520
24,275
10,117
9,392
22,973
10,080
6,315
47,327
4,703
Peduncle
Pinnule
Rachis
Whole animal
B
log10FPKM
C
High expression (log2FoldChange > 1 ,FDR <= 0.001)
Low expression (log2FoldChange < -1 ,FDR <= 0.001)
2,368
7,386
1,293
2,539
1,818
6,316
Pinnule VS Peduncle
Pinnule VS Rachis
Rachis VS Peduncle
D
Translation elongation factor (GO:0003746)
Ribonucleoprotein complex binding (GO:0043021)
Protein kinase activator (GO:0030295)
Actin monomer binding (GO:0003785)
DNA-endonuclease (GO:0003906)
Damaged DNA binding (GO:0003684)
Zinc ion binding (GO:0008270)
Metal ion binding (GO:0046872)
ATP binding (GO:0005524)
RNA binding (GO:0003723,GO:0003729,GO:0019843)
GTP binding (GO:0005525)
GTPase (GO:0003924)
Structural constituent of ribosome (GO:0003735)
Most Expressed in Peduncle
GTP binding
Ribonucleoprotein complex binding
Protein kinase activator
DNA-endonuclease
Damaged DNA binding
Metal ion binding
ATP binding
RNA binding
GTPase
Structural constituent of ribosome
Most Expressed in Pinnula
Translation elongation factor
Ribonucleoprotein complex binding
Protein kinase activator
DNA-endonuclease
Damaged DNA binding
Metal ion binding
ATP binding
RNA binding
GTP binding
GTPase
Structural constituent of ribosome
Most Expressed in Rachis
E
RNA polymerase II cis-regulatory region sequence-specific DNA binding (GO:0000978)
Structural constituent of ribosome
Ribonucleoprotein complex binding
DNA-binding transcription factor activity, RNA pol.II-specific (GO:0000981)
Protein kinase activator
ECM structural constituent conferring tensile strength (GO:0030020)
Nutrient reservoir activity (GO:0045735)
Ferroxidase (GO:0004322)
Ferrous iron binding (GO:0008198)
Ferric iron binding (GO:0008199)
Metal ion binding
Most Expressed
F
Serine-type endopeptidase (GO:0004252)
Metalloendopeptidase activity (GO:0004222)
Calcium ion binding (GO:0005509)
Oxidoreductase (GO:0016702)
Metal ion binding (GO:0046872)
Zinc ion binding (GO:0008270)
Pinnule VS Peduncle
Sequence-specific DNA binding (GO:0043565)
Cytochrome-c oxidase (GO:0004129)
RNA binding (GO:0003723)
Hydrolase (GO:0016787)
Copper ion binding (GO:0005507)
Serine-type endopeptidase
Protein serine/threonine kinase (GO:0004674)
Cysteine-type endopeptidase (GO:0004197)
Pinnule VS Rachis
Protein heterodimerization (GO:0046982)
Nucleic acid binding (GO:0003677,GO:003676)
Calcium ion binding
Channel (GO:0015267)
Serine-type endopeptidase
Toxin (GO:0090729)
Metal ion binding
Oxidoreductase
Zinc ion binding
Rachis VS Peduncle

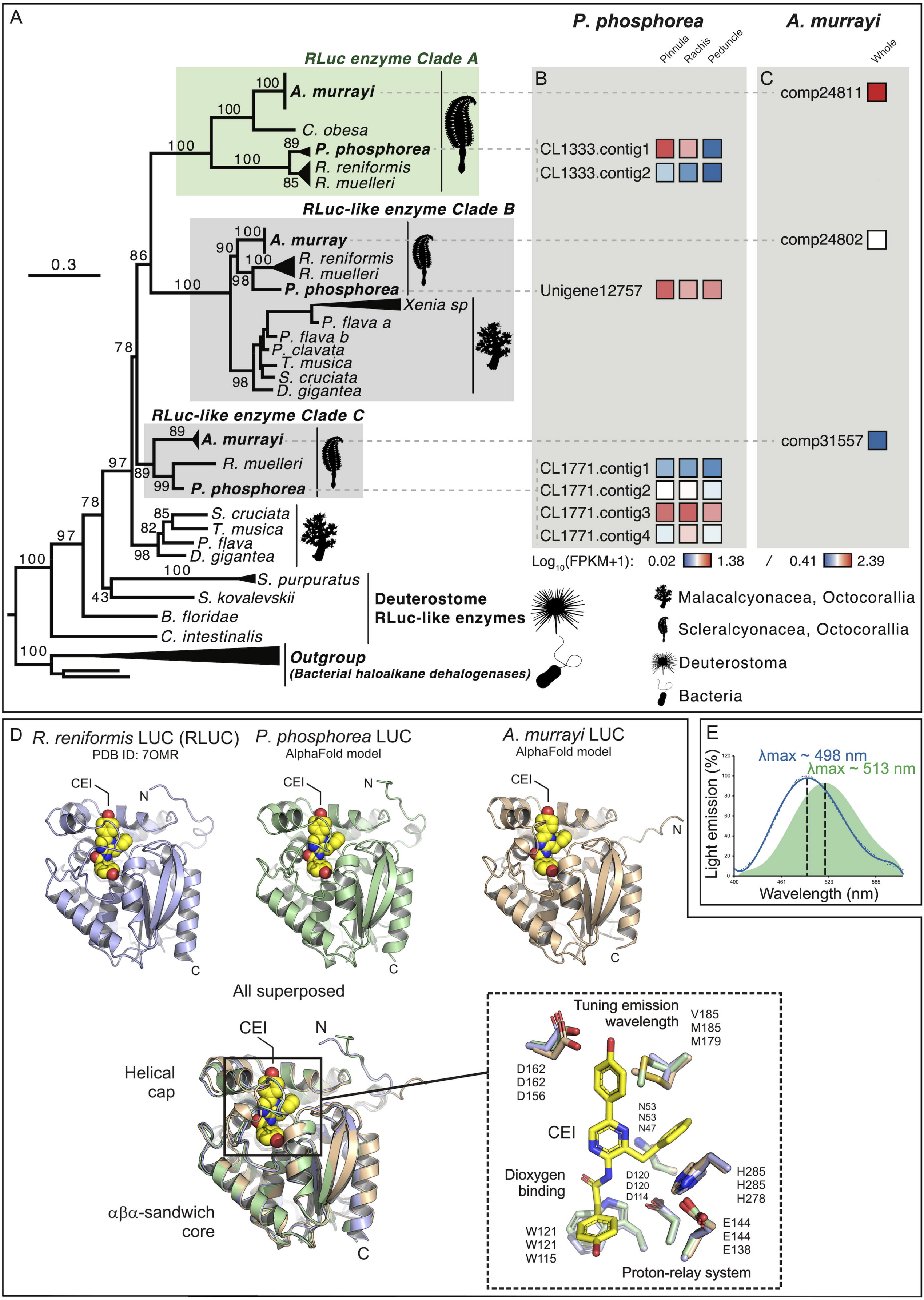
A
P. phosphorea
A. murrayi
Pinnula
Rachis
Peduncle
Whole
RLuc enzyme Clade A
A. murrayi
C. obesa
P. phosphorea
R. reniformis
R. muelleri
RLuc-like enzyme Clade B
A. murray
R. reniformis
R. muelleri
P. phosphorea
Xenia sp
P. flava a
P. flava b
P. clavata
T. musica
S. cruciata
D. gigantea
RLuc-like enzyme Clade C
A. murrayi
R. muelleri
P. phosphorea
S. cruciata
T. musica
P. flava
D. gigantea
S. purpuratus
S. kovalevskii
B. floridae
C. intestinalis
Outgroup
(Bacterial haloalkane dehalogenases)
Deuterostome
RLuc-like enzymes
0.3
B
CL1333.contig1
CL1333.contig2
Unigene12757
CL1771.contig1
CL1771.contig2
CL1771.contig3
CL1771.contig4
C
comp24811
comp24802
comp31557
Log10(FPKM+1): 0.02 1.38 / 0.41 2.39
Malacalcyonacea, Octocorallia
Scleralcyonacea, Octocorallia
Deuterostoma
Bacteria
D
R. reniformis LUC (RLUC)
PDB ID: 7OMR
P. phosphorea LUC
AlphaFold model
A. murrayi LUC
AlphaFold model
CEI
N
C
All superposed
Helical cap
αβα-sandwich core
Tuning emission wavelength
V185
M185
M179
D162
D162
D156
N53
N53
N47
CEI
Dioxygen binding
D120
D120
D114
H285
H285
H278
W121
W121
W115
E144
E144
E138
Proton-relay system
E
λmax ~ 498 nm
λmax ~ 513 nm
Light emission (%)
Wavelength (nm)

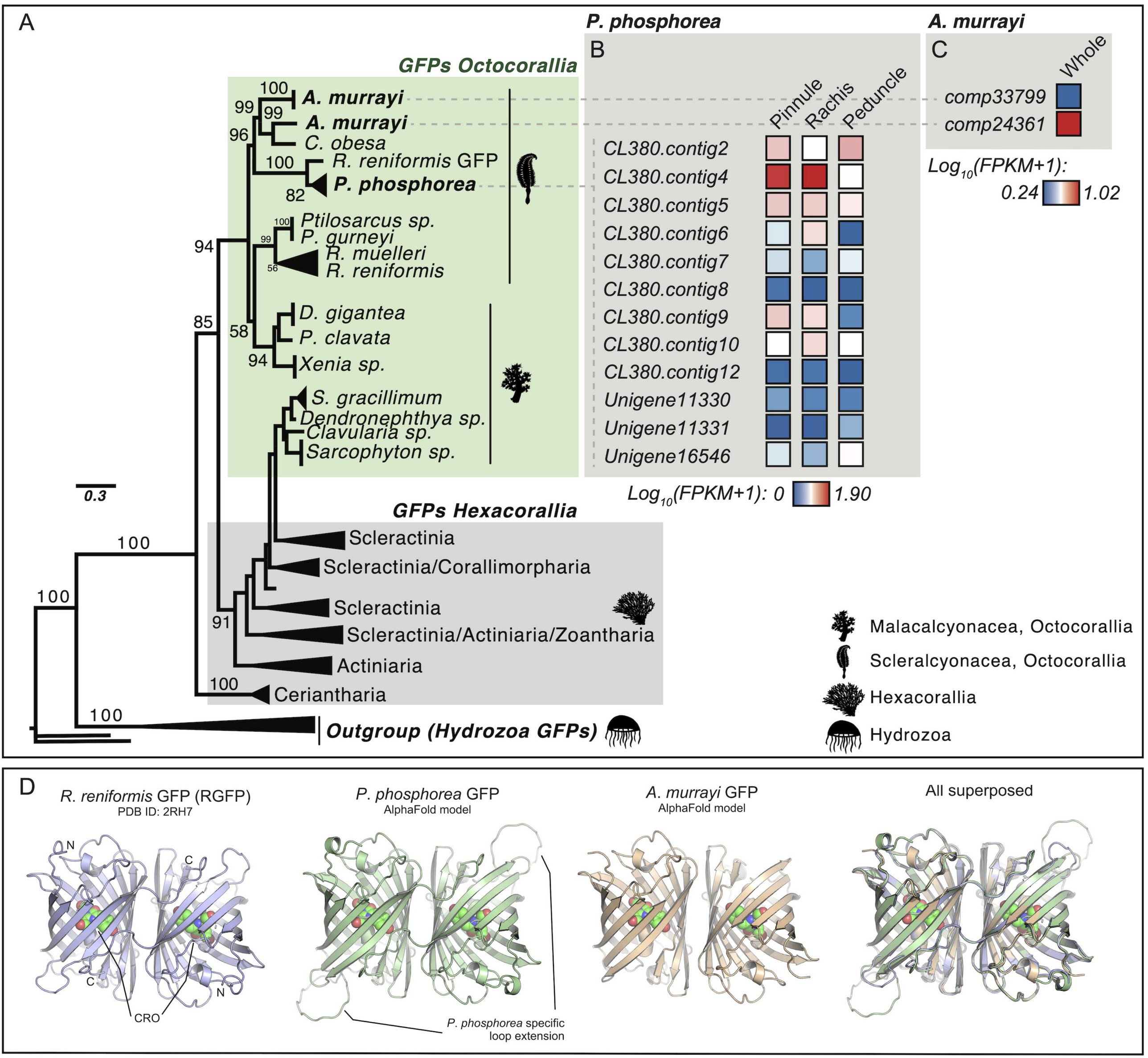
A
GFPs Octocorallia
A. murrayi
A. murrayi
C. obesa
R. reniformis GFP
P. phosphorea
Ptilosarcus sp.
P. gurneyi
R. muelleri
R. reniformis
D. gigantea
P. clavata
Xenia sp.
S. gracillimum
Dendronephthya sp.
Clavularia sp.
Sarcophyton sp.
0.3
GFPs Hexacorallia
Scleractinia
Scleractinia/Corallimorpharia
Scleractinia
Scleractinia/Actiniaria/Zoantharia
Actiniaria
Ceriantharia
Outgroup (Hydrozoa GFPs)
P. phosphorea
B
Pinnule
Rachis
Peduncle
CL380.contig2
CL380.contig4
CL380.contig5
CL380.contig6
CL380.contig7
CL380.contig8
CL380.contig9
CL380.contig10
CL380.contig12
Unigene11330
Unigene11331
Unigene16546
Log10(FPKM+1): 0
1.90
A. murrayi
C
Whole
comp33799
comp24361
Log10(FPKM+1):
0.24
1.02
Malacalcyonacea, Octocorallia
Scleralcyonacea, Octocorallia
Hexacorallia
Hydrozoa
D
R. reniformis GFP (RGFP)
PDB ID: 2RH7
N
C
C
N
CRO
P. phosphorea GFP
AlphaFold model
P. phosphorea specific loop extension
A. murrayi GFP
AlphaFold model
All superposed

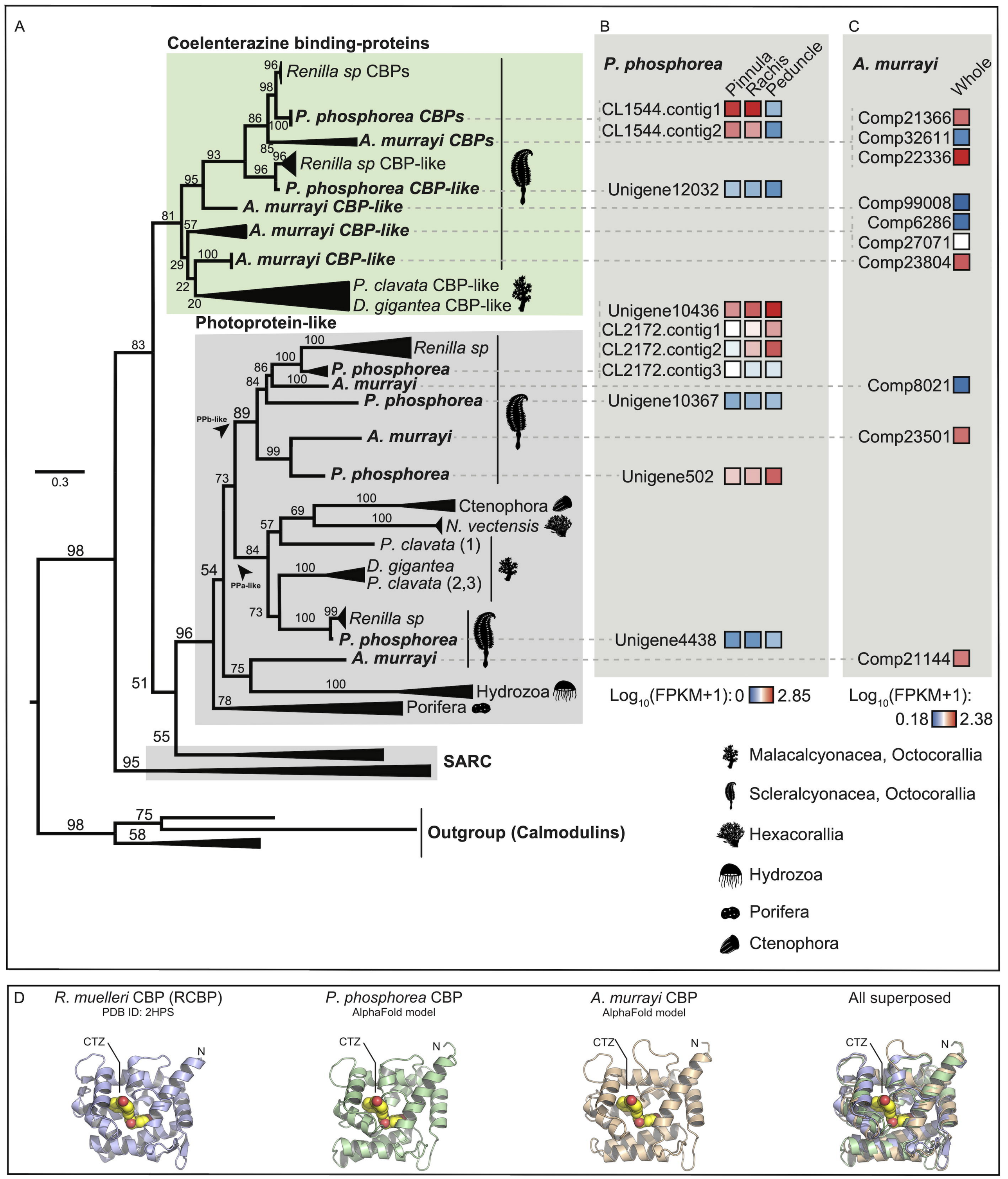
A
Coelenterazine binding-proteins
Renilla sp CBPs
P. phosphorea CBPs
A. murrayi CBPs
Renilla sp CBP-like
P. phosphorea CBP-like
A. murrayi CBP-like
A. murrayi CBP-like
A. murrayi CBP-like
P. clavata CBP-like
D. gigantea CBP-like
Photoprotein-like
Renilla sp
P. phosphorea
A. murrayi
P. phosphorea
PPb-like
A. murrayi
P. phosphorea
Ctenophora
N. vectensis
P. clavata (1)
D. gigantea
P. clavata (2,3)
PPa-like
Renilla sp
P. phosphorea
A. murrayi
Hydrozoa
Porifera
SARC
Outgroup (Calmodulins)
0.3
B
P. phosphorea
Pinnula
Rachis
Peduncle
CL1544.contig1
CL1544.contig2
Unigene12032
Unigene10436
CL2172.contig1
CL2172.contig2
CL2172.contig3
Unigene10367
Unigene502
Unigene4438
Log10(FPKM+1): 0 2.85
C
A. murrayi
Whole
Comp21366
Comp32611
Comp22336
Comp99008
Comp6286
Comp27071
Comp23804
Comp8021
Comp23501
Comp21144
Log10(FPKM+1): 0.18 2.38
Malacalcyonacea, Octocorallia
Scleralcyonacea, Octocorallia
Hexacorallia
Hydrozoa
Porifera
Ctenophora
D
R. muelleri CBP (RCBP)
PDB ID: 2HPS
P. phosphorea CBP
AlphaFold model
A. murrayi CBP
AlphaFold model
All superposed
CTZ
N

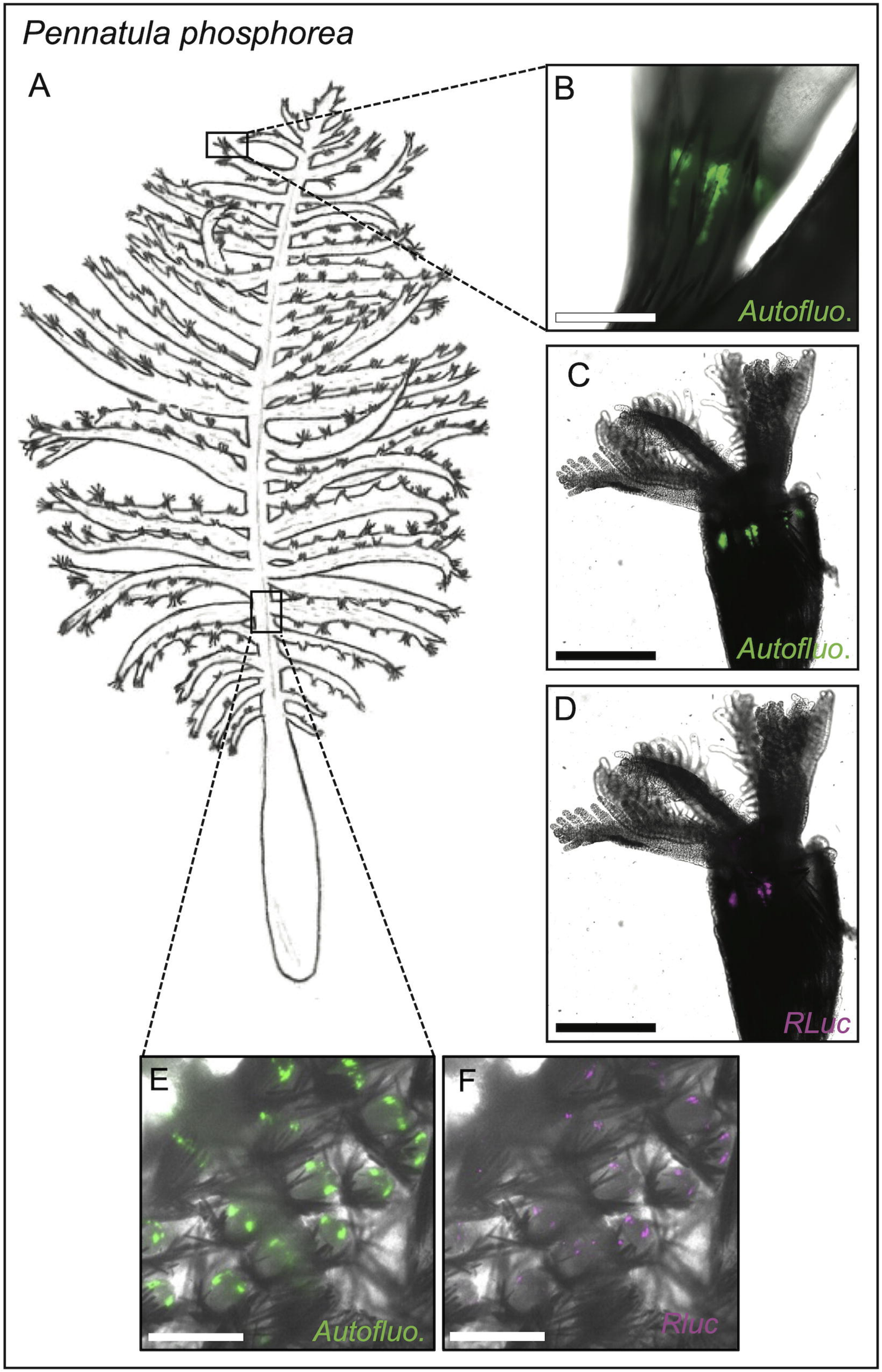
Pennatula phosphorea
A
B
Autofluo.
C
Autofluo.
D
RLuc
E
Autofluo.
F
Rluc

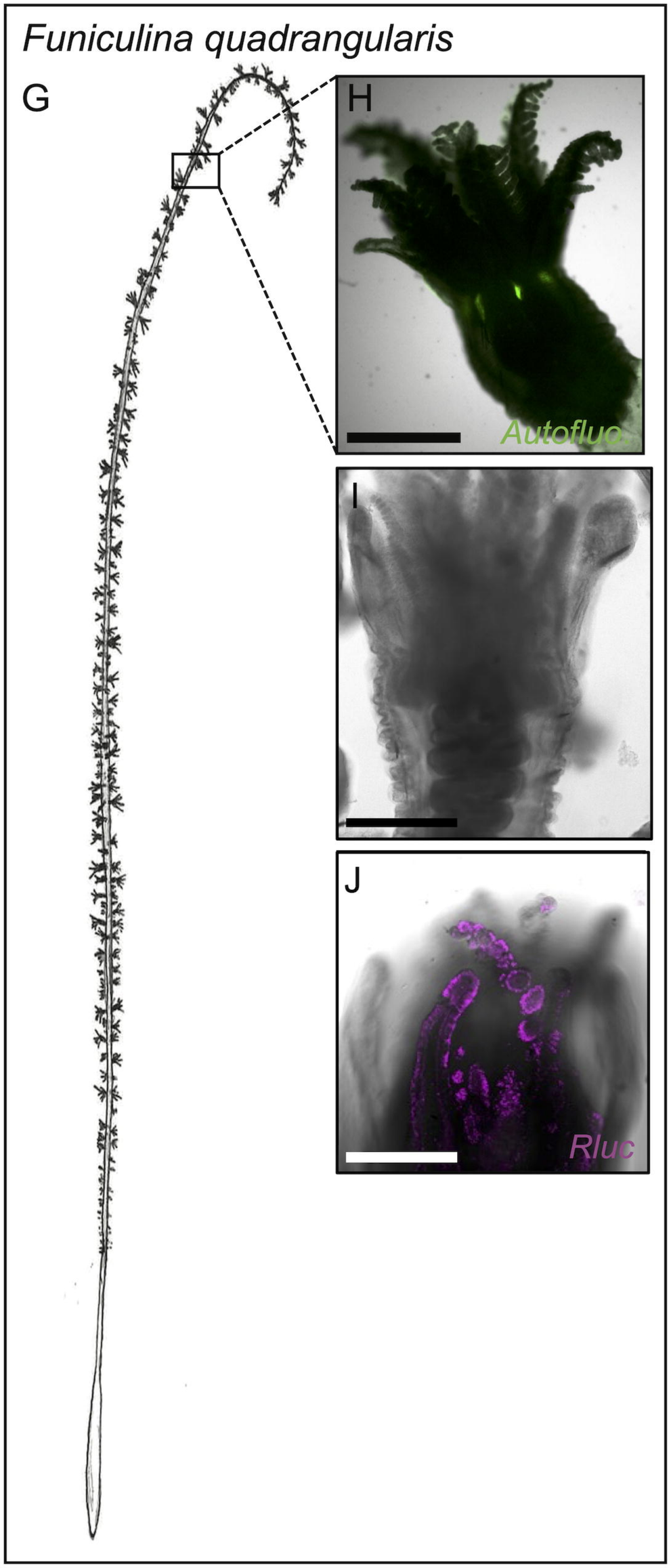
Funiculina quadrangularis
G
H
Autofluo.
I
J
Rluc

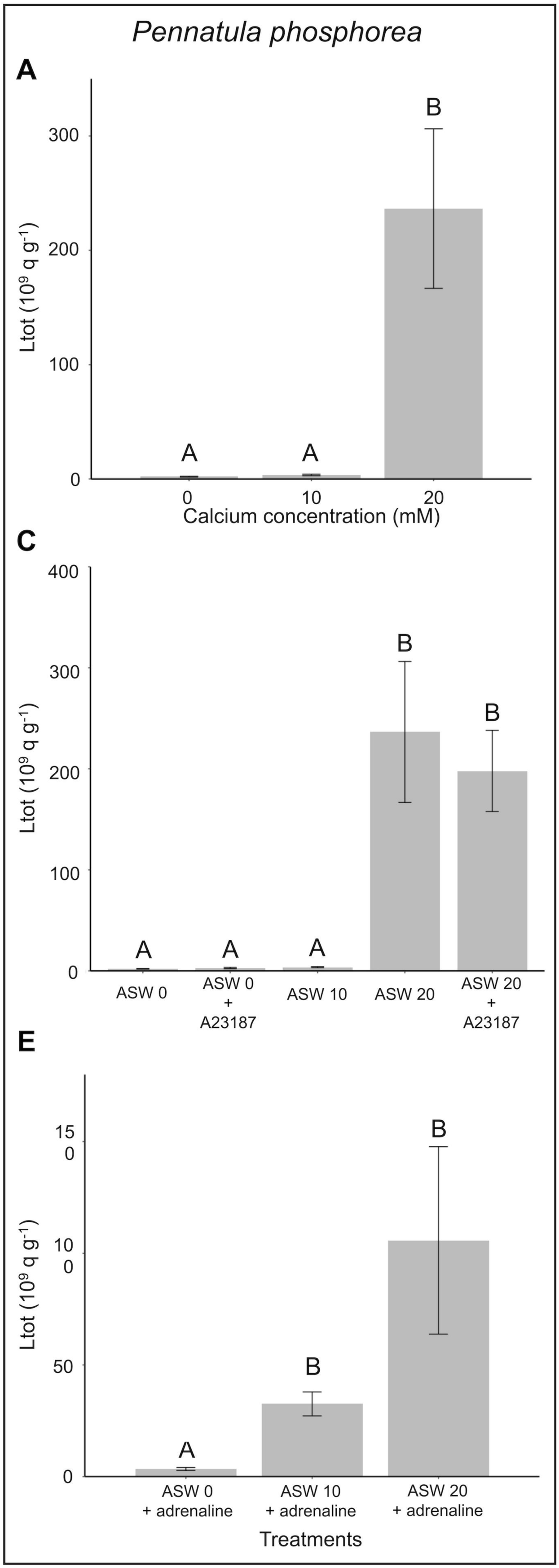
Pennatula phosphorea
A
Ltot (10^9 q g^{-1})
300
200
100
0
A
A
B
0
10
20
Calcium concentration (mM)
C
400
300
200
100
0
A
A
A
B
B
ASW 0
ASW 0 + A23187
ASW 10
ASW 20
ASW 20 + A23187
E
15 0
10 0
50
0
A
B
B
ASW 0 + adrenaline
ASW 10 + adrenaline
ASW 20 + adrenaline
Treatments

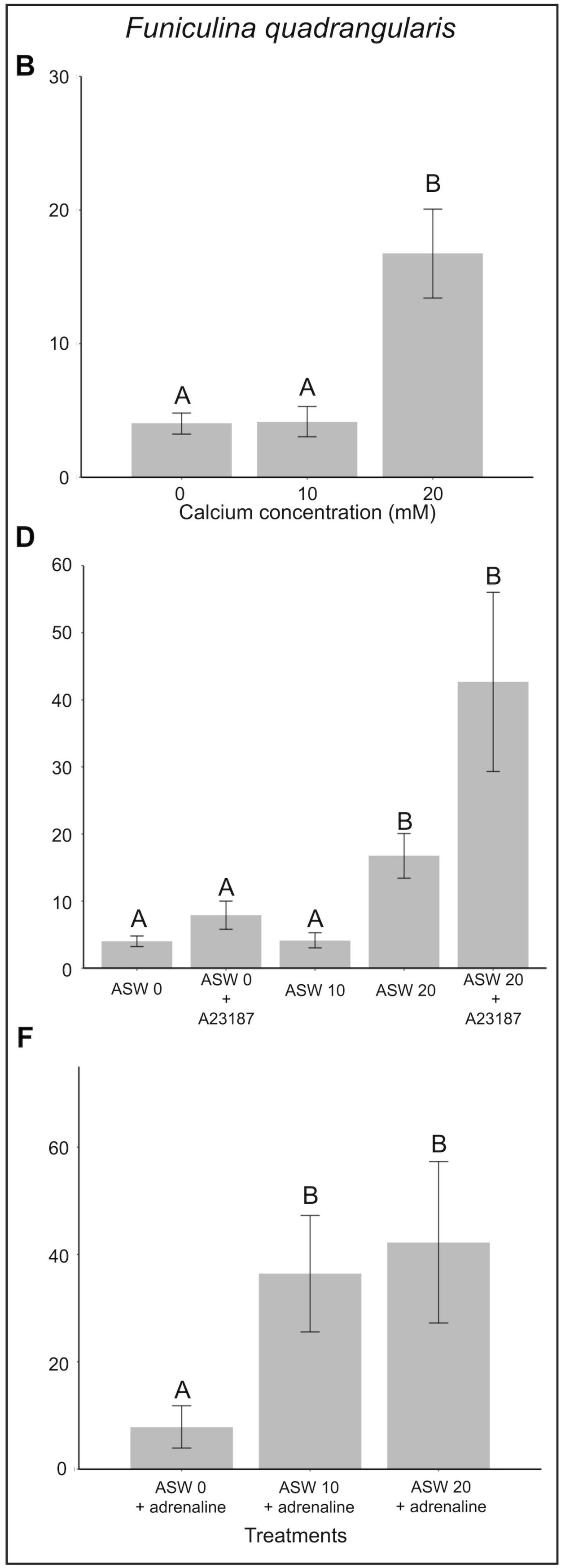
Funiculina quadrangularis
B
30
20
10
0
A
A
B
0
10
20
Calcium concentration (mM)
D
60
50
40
30
20
10
0
A
A
A
B
B
ASW 0
ASW 0 + A23187
ASW 10
ASW 20
ASW 20 + A23187
F
60
40
20
0
A
B
B
ASW 0 + adrenaline
ASW 10 + adrenaline
ASW 20 + adrenaline
Treatments

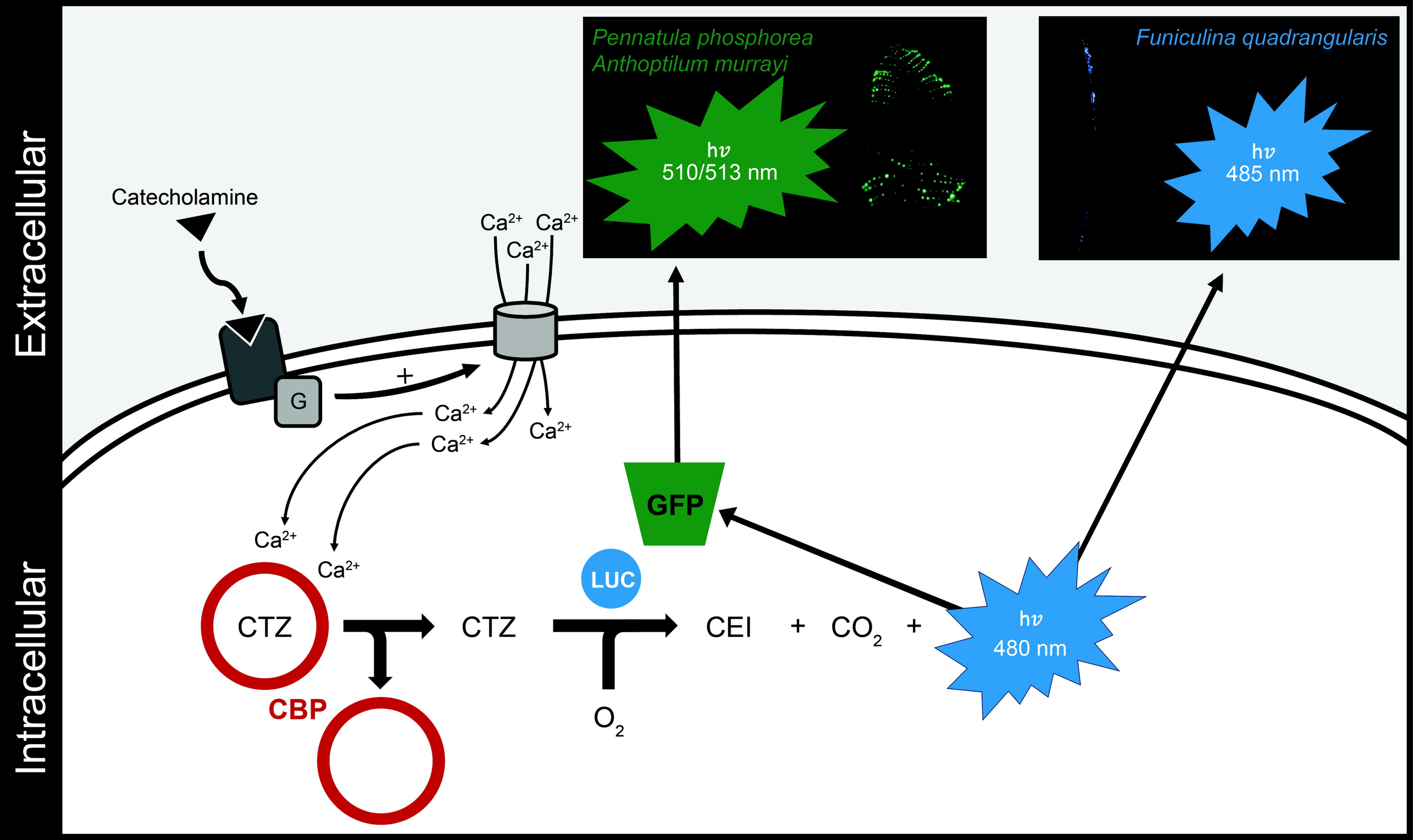
Extracellular
Intracellular
Pennatula phosphorea
Anthoptilum murrayi
hν
510/513 nm
Funiculina quadrangularis
hν
485 nm
Catecholamine
G
+
Ca2+
Ca2+
Ca2+
Ca2+
Ca2+
Ca2+
Ca2+
Ca2+
GFP
LUC
CTZ
CTZ
CEI
+
CO2
+
hν
480 nm
O2
CBP